2023

Status and Future Plans for C³ R&D

Emilio A. Nanni

Martin Breidenbach

Zenghai Li

Caterina Vernieri

Faya Wang

See next page for additional authors

Original Publication Citation

Nanni, E. A., Breidenbach, M., Li, Z., Vernieri, C., Wang, F., White, G., Bai, M., Belomestnykh, S., Bhat, P., Barklow, T., Berg, W. J., Borzenets, V., Byrd, J., Dhar, A., Dhuley, R. C., Doss, C., Duris, J., Edelen, A., Emma, C., . . . Wootton, K. P. (2023). Status and future plans for C3 R&D. *Journal of Instrumentation*, *18*(9), 1-50, Article P09040. https://doi.org/10.1088/1748-0221/18/09/P09040

Published by IOP Publishing for Sissa Medialab

Received: *June 2, 2023*
Accepted: *August 23, 2023*
Published: *September 28, 2023*

Snowmass'2021 Accelerator Frontier

Status and future plans for C^3 R&D

Emilio A. Nanni,[g,*] **Martin Breidenbach,**[g] **Zenghai Li,**[g] **Caterina Vernieri,**[g] **Faya Wang,**[g] **Glen White,**[g] **Mei Bai,**[g] **Sergey Belomestnykh,**[c,h] **Pushpalatha Bhat,**[c] **Tim Barklow,**[g] **William J. Berg,**[a] **Valery Borzenets,**[g] **John Byrd,**[a] **Ankur Dhar,**[g] **Ram C. Dhuley,**[c] **Chris Doss,**[j] **Joseph Duris,**[g] **Auralee Edelen,**[g] **Claudio Emma,**[g] **Josef Frisch,**[g] **Annika Gabriel,**[g] **Spencer Gessner,**[g] **Carsten Hast,**[g] **Chunguang Jing,**[a] **Arkadiy Klebaner,**[g] **Dongsung Kim,**[e] **Anatoly K. Krasnykh,**[g] **John Lewellen,**[e] **Matthias Liepe,**[b] **Michael Litos,**[j] **Xueying Lu,**[a] **Jared Maxson,**[b] **David Montanari,**[c] **Pietro Musumeci,**[i] **Sergei Nagaitsev,**[k,l] **Alireza Nassiri,**[a] **Cho-Kuen Ng,**[g] **Mohamed A.K. Othman,**[g] **Marco Oriunno,**[g] **Dennis Palmer,**[g] **J. Ritchie Patterson,**[b] **Michael E. Peskin,**[g] **Thomas J. Peterson,**[g] **John Power,**[a] **Ji Qiang,**[d] **James Rosenzweig,**[i] **Vladimir Shiltsev,**[c] **Muhammad Shumail,**[g] **Evgenya Simakov,**[e] **Emma Snively,**[g] **Bruno Spataro,**[f] **Sami Tantawi,**[g] **Harry van der Graaf,**[m] **Brandon Weatherford,**[g] **Juhao Wu**[g] **and Kent P. Wootton**[a]

[a] *Argonne National Laboratory, 9700 S Cass Ave., Lemont, IL, U.S.A.*
[b] *Cornell University, 616 Thurston Ave., Ithaca, NY, U.S.A.*
[c] *Fermi National Accelerator Laboratory, PO Box 500, Batavia, IL, U.S.A.*
[d] *Lawrence Berkeley National Laboratory, 1 Cyclotron Rd, Berkeley, CA, U.S.A.*
[e] *Los Alamos National Laboratory, 1450 Central Ave., Los Alamos, NM, U.S.A.*
[f] *National Laboratory of Frascati, INFN-LNF, Via Enrico Fermi, 54, 00044 Frascati, Italy*
[g] *SLAC National Accelerator Laboratory, Stanford University, 2575 Sand Hill Rd, Menlo Park, CA, U.S.A.*
[h] *Department of Physics and Astronomy, Stony Brook University, 100 Nicolls Rd, Stony Brook, NY, U.S.A.*
[i] *Department of Physics, University of California, Los Angeles, 405 Hilgard Avenue, Los Angeles, CA, U.S.A.*
[j] *Department of Physics, University of Colorado, Boulder, 20 UCB, Boulder, CO, U.S.A.*
[k] *Thomas Jefferson National Accelerator Facility, Old Dominion University, 12000 Jefferson Ave, Newport News, VA, U.S.A.*
[l] *Department of Physics, Old Dominion University, 5115 Hampton Blvd, Norfolk, VA, U.S.A.*
[m] *National Institute for Subatomic Physics, Nikhef, Science Park 105, 1098 XG Amsterdam, Netherlands*

E-mail: nanni@slac.stanford.edu

Abstract: C^3 is an opportunity to realize an e^+e^- collider for the study of the Higgs boson at $\sqrt{s}$ = 250 GeV, with a well defined upgrade path to 550 GeV while staying on the same short facility footprint [2, 3]. C^3 is based on a fundamentally new approach to normal conducting linear accelerators that achieves both high gradient and high efficiency at relatively low cost. Given the

*Corresponding author.

https://doi.org/10.1088/1748-0221/18/09/P09040

2023 JINST 18 P09040

advanced state of linear collider designs, the key system that requires technical maturation for C^3 is the main linac. This paper presents the staged approach towards a facility to demonstrate C^3 technology with both Direct (source and main linac) and Parallel (beam delivery, damping ring, ancillary component) R&D.

The primary goal of the C^3 Demonstration R&D Plan is to reduce technical and cost risk by building and operating the key components of C^3 at an adequate scale. This R&D plan starts with the engineering design, and demonstration of one cryomodule and will culminate in the construction of a 3 cryomodule linac with pre-production prototypes. This R&D program would also demonstrate the linac rf fundamentals including achievable gradient and gradient stability over a full electron bunch train and breakdown rates. It will also investigate beam dynamics including energy spread, wakefields, and emittance growth. This work will be critical to confirm the suitability of the C^3 beam parameters for the physics reach and detector performance in preparation for a Conceptual Design Report (CDR), as well as for follow-on technology development and industrialization.

The C^3 Demonstration R&D Plan will open up significant new scientific and technical opportunities based on development of high-gradient and high-efficiency accelerator technology. It will push this technology to operate both at the GeV scale and mature the technology to be reliable and provide high-brightness electron beams.

The timeline for progressing with C^3 technology development will be governed by practical limitations on both the technical progress and resource availability. It consists of four stages: Stage 0) Ongoing fundamental R&D on structure prototypes, damping and vibrations. Stage 1) Advancing the engineering maturity of the design and developing start-to-end simulations including space-charge and wakefield effects. This stage will include testing of strucutres operating at cryogenic temperatures. Beam tests would be performed with high beam current to test full beam loading. Stage 2) Production and testing of the first cryomodule at cryogenic temperatures. This would provide sufficient experimental data to compile a CDR and it is anticipated for Stage 2 to last 3 years and to culminate with the transport of photo-electrons through the first cryomodule. Stage 3) Updates to the engineering design of the cryomodules, production of the second and third cryomodule and their installation. Lower charge and lower emittance beams will be used to investigate emittance growth. The successful full demonstration of the 3 cryomodules to deliver up to a 3 GeV beam and achieve the C^3five gradient will allow a comprehensive and robust evaluation of the technical design of C^3 as well as mitigate technical, schedule, and cost risks required to proceed with a Technical Design Report (TDR).

KEYWORDS: Acceleration cavities and superconducting magnets (high-temperature superconductor, radiation hardened magnets, normal-conducting, permanent magnet devices, wigglers and undulators); Accelerator Applications; Accelerator modelling and simulations (multi-particle dynamics, single-particle dynamics); Accelerator Subsystems and Technologies

Contents

2023 JINST 18 P09040

1 Introduction

A top priority for the global particle physics community is to carry out precision studies of the Higgs boson using an e^+e^- collider. In this article, we present a the R&D needed for a new proposal for such a collider based on recent advances in the technology of cold copper distributed coupling accelerators. Distributed coupling is a novel form of power distribution in the RF accelerator that allows for increased accelerator performance and better optimization. Cold copper refers to the operation of the accelerator at cryogenic temperatures to increase RF efficiency and the achievable accelerating gradient. These new technologies are described by the acronym C^3, or "Cool Copper Collider" [1–5]. Specifically, we propose a C^3 linear collider on an 8 km footprint. This collider can reach 250 GeV in the center of mass energy (CM) using innovative technologies, with the possibility of a relatively inexpensive upgrade to 550 GeV on the same footprint. This will achieve the goals of precision Higgs boson and top quark measurements and it will at the same time provide a basis for the extension of e^+e^- physics into the multi-TeV energy range.

A facility of this type is urgently needed by the particle physics community. The urgency grows out of the great success of particle physics over the past 30 years which, paradoxically, has led to increasing uncertainty about its future.

To address this situation, our community needs to put forward an ambitious program to discover the now-unknown fundamental interactions that underlie the SM. The community [6–11] is converging globally on a program with two essential elements:

1. Construction of an e^+e^- Higgs factory: among all of the SM particles, the Higgs boson is the most central, the most tightly connected to the mysteries of the model and, at the same time, the particle least well studied. With a next-generation e^+e^- collider, it will be possible to measure the properties of the Higgs boson to the 1% level and below, a level that allows the discovery of effects from models beyond the SM. Several alternative technologies allow the construction of an e^+e^- Higgs factory within 15 years, but this also requires a willing national host and a strong push from our global community.

2. Development of multiple routes to an affordable multi-TeV collider: the first expectation for the energy scale of the new fundamental forces was the 1 TeV scale of Higgs boson physics. From the LHC experiments, we now see that (barring some special scenarios) this physics is most likely to appear at a higher energy scale. On the other hand, that scale cannot be orders of magnitude higher than 1 TeV if we expect to have a physics explanation for the Higgs field and its vacuum value. Reaching parton-parton CM energies of order 10 TeV should be the next goal. This goal is not realizable with any current technology. Cost and power consumption are major issues, with drastic differences across collider concepts [12]. We need to study as many feasible routes as possible, so that at least one route can succeed.

For the first of these elements, the leading candidate now is the International Linear Collider (ILC) in Japan [13]. The technical design is virtually complete, and the technology is mature. Still, there remains the question of whether Japan will offer to host this project. On a longer time line, the Future Circular Collider (FCC) electron-positron stage may provide a solution [14]. But this depends on funding the needed 100 km tunnel, which costs as much as the LHC and brings no

2023 JINST 18 P09040

physics capability in itself. The Circular Electron-Positron Collider (CEPC) in China may provide another possible solution [15, 16]. As opposed to linear machines, circular colliders are strongly limited by synchrotron radiation above 350– 400 GeV center of mass energy.

For the second of these elements, ideas are being pursued based on proton-proton colliders with high-field magnets [17], muon colliders [18, 19], and plasma-wakefield electron accelerators [20, 21]. The proton-proton route now seems feasible but with a very high cost; the other routes have technical barriers to overcome. These very high energy options will require significant time and R&D to realize.

The development of cold copper distributed coupling accelerating cavities can provide an alternative route to achieve both steps in this program. Our optimism about the capabilities of optimized copper accelerating cavities is based on new design ideas detailed in [4, 5]. The most important problem for operation of a normal-conducting cavity at high fields is electrical breakdown. Cavities optimized for efficiency, high accelerating gradient and low breakdown have small irises that prevent power flow at the fundamental frequency. Individual feeds to each cavity from a common RF manifold, all in the same copper block, solve this problem. Modern numerically controlled manufacturing techniques can build appropriate manifolds and individual cavity feeds in an extremely cost-effective way. We have also discovered that operation of these cavities at 80 K increases their material strength and conductivity, giving marked improvements in performance. These two innovations lead to the C^3 concept, a new elevated baseline for normal-conducting electron accelerators [2, 3].

Although there is no engineered and costed design for a 250 GeV e^+e^- C^3 yet, this proposal is based on the SLC experience at SLAC and the extensive design work for ILC and CLIC [96, 97]. C^3 adds significant capabilities that allow robust designs with an accelerating gradient of 120 MeV/m.

This linac technology could be extended up to a 3 TeV collider by some combination of raising the gradient and extending the machine. The primary challenges for the linac in the multi-TeV range are the cost and required power. These can be mitigated by highly efficient, low-cost RF power sources that are now being developed. Additionally, beyond 1 TeV beam-beam interactions increase the challenges associated with the beam delivery system and final focus. Beyond 3 TeV we enter *terra incognita*. Here futuristic concepts such as muon colliders [18, 19] or plasma wakefield accelerators [20, 21] may be required.

R&D on the C^3 concept is already being pursued at SLAC, UCLA, INFN, LANL and Radiabeam, along with closely related research in high gradient RF acceleration with CERN, KEK, PSI, MIT, and many other partners in the high gradient research community [22]. There is direct synergy with the development of compact electron accelerators for medical applications [23–26] and the creation of compact X-ray free electron lasers [27, 29, 31] (FELs). This technology will be further developed, and it is expected to meet many of its initial goals within the Snowmass and P5 timelines, using our current resources. The development of accelerators at the 100 GeV scale and higher will require dedicated resources from HEP.

Given the advanced state of linear collider designs, the key system that requires technical maturation for C^3 is the main linac. We are pursuing R&D that will culminate in the construction of a 3 cryomodule linac with the cryomodules being pre-production prototypes.

The completion of the C^3 demonstration R&D program would demonstrate:

- the linac rf fundamentals including achievable gradient and gradient stability over a full electron bunch train and breakdown rates

2023 JINST 18 P09040

- beam dynamics including energy spread, wakefields, and emittance growth
- cooling performance under liquid nitrogen (LN_2) with direct measurements of vibrations from several accelerators fitted with sensitive cryogenic accelerometers
- small quantity component costs providing a reliable basis for extrapolation to C^3 scale production
- prototype assembly tooling and exploration of industrial production and assembly
- module-to-module assembly, possibly of simple robotic welding for cryostat connections

The C^3 Demonstration R&D Plan will open up significant new scientific and technical opportunities based on development of high-gradient and high-efficiency accelerator technology. Accelerator technology that forms the basis of C^3 is presently being pursued and developed for multiple small-scale accelerator projects. The C^3 Demonstration R&D Plan will push this technology to operate both at the GeV level and mature the technology to be reliable and provide high-brightness electron beams. The rf photo-injector for the demonstration could be a new design based on the recent advances in cryogenic copper technology with significantly higher peak field at the emission surface. These GeV-class high-brightness beams produced as part of the C^3 demonstration plan could be utilized for a variety of follow-on experiments targeting HEP applications, for beam physics studies, advanced accelerator concepts (plasma-wakefield staging, plasma lenses), positron target development, exploring novel concepts in generation of polarized beams, and developing advanced techniques for machine control with AI/ML. Already with GeV-class high-brightness beams many applications outside of HEP would be directly impacted by C^3 technology. For example, FEL, gamma-ray or x-ray inverse Compton sources could be developed. The high-brightness high-charge electron source could be utilized for ultra-fast electron diffractometry/microscopy or incorporated as a new electron source for existing x-ray FELs to push pulse energy, x-ray energy or repetition rate.

2 Current and near-future R&D on C^3 accelerator technology

2.1 New design ideas for normal conducting accelerators

The C^3 structure grew from a study of the fundamental limitations of high accelerating gradients and breakdown in normal conductors. Major improvements in fields and breakdown rates are possible with an optimized cavity shape that limits peak surface electric and magnetic fields, but with the seemingly problematic feature of an iris too small to propagate the fundamental RF mode. This led to the idea of an easily fabricated RF manifold and distributed coupling machined from the same blocks of metal as the accelerator. The distributed coupling powers the cavities at the correct phase and with equal fractions of RF power. Developing this idea led to the two major advances:

1. RF power can be distributed to the cells of a copper accelerator individually through a distributed coupling waveguide. With optimized cavity geometries, this scheme allows us to efficiently power the cells while maintaining strict limits on peak surface electric and magnetic fields. A diagram of the structure's vacuum space is shown in figure 1. The structure can be mass-produced efficiently with currently used techniques.

2023 JINST 18 P09040

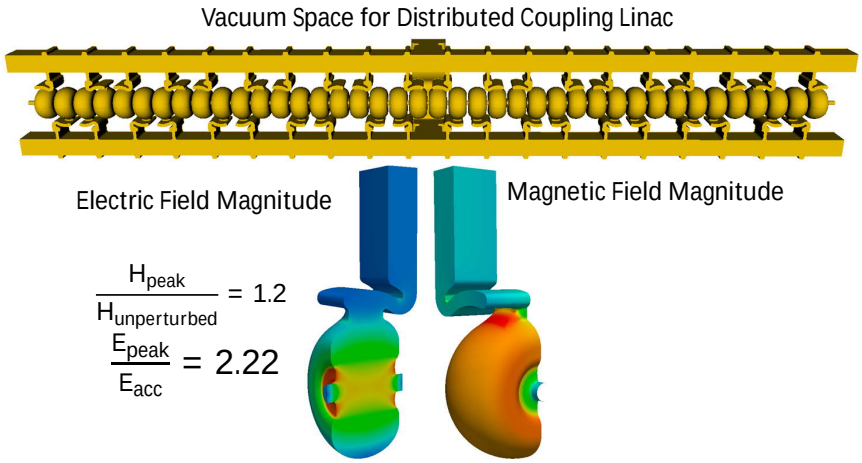

Figure 1. (top) Vacuum space for a one meter long 40-cell C-band accelerating structure operating in the π mode. (bottom) The magnitude of the electric and magnetic field in each cavity. Cavity geometries were optimized to limit the electric and magnetic fields strengths. The peak surface electric field to accelerating gradient ratio is 2.22 (266 MV/m for a 120 MeV/m gradient). The perturbation to the magnetic field from the RF coupler increases the peak magnetic field by 1.2. For a gradient of 120 MeV/m the peak magnetic field in the coupler is 0.372 MA/m.

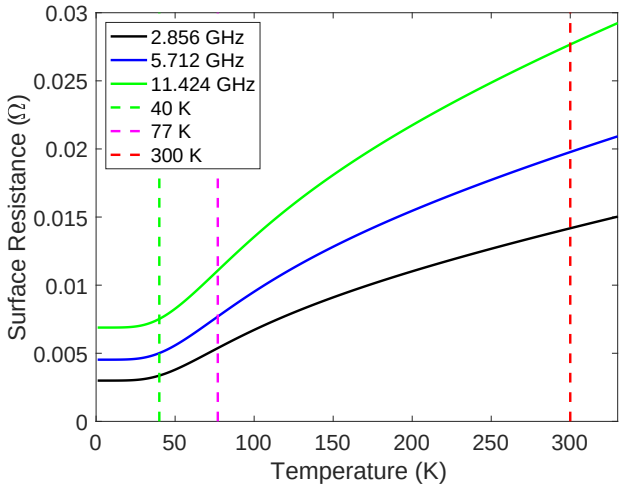

Figure 2. Surface resistance of copper as a function of temperature including the anomalous skin effect. The reduction for surface resistance at 77 K and 5.712 GHz (C-band) is a factor 2.55 compared to 300 K. [88, 89].

2. Operating a copper structure at cryogenic temperatures allows us to further reduce RF power requirements while increasing the achievable beam loading and accelerating gradient, through a combination of increased material strength and reduced strain. A key parameter, the surface resistance, is shown as a function of temperature in figure 2. Almost all of the improvement is achieved by operation at liquid nitrogen temperature, 77 K.

The result of these two advances is a reduction in the required RF power to establish the gradient by greater than a factor of six compared to other normal conducting accelerators with similar beam

2023 JINST 18 P09040

aperture, see table 1. The RF to beam power efficiency increases significantly to 45% and plays an important role in the feasibility of extending C^3 to the multi-TeV scale. The achievable accelerating gradient also increases. The full collider design [3] has a gradient of 120 MeV/m, but this number is not limited by the accelerator technology, but rather by an overall optimization with the cost of RF power. The overall power consumption, see table 1, is competitive with other collider concepts [28] and provides sustainable pathway to building and operating a Higgs factory [30].

Table 1. Beam parameters for C^3.

CM Energy [GeV]	250	550
Luminosity [$\times 10^{34}$/cm^{2}s]	1.3	2.4
Gradient [MeV/m]	70	120
Effective Gradient [MeV/m]	63	108
Length [km]	8	8
Num. Bunches per Train	133	75
Train Rep. Rate [Hz]	120	120
Bunch Spacing [ns]	5.26	3.5
Bunch Charge [nC]	1	1
Strucutre Aperture [mm]	3.55	3.55
Crossing Angle [rad]	0.014	0.014
Site Power [MW]	$\sim$ 150	$\sim$ 175

RF accelerators can operate over a wide range of frequencies. Most RF accelerators developed for a linear collider operate between 1–12 GHz. A detailed study of cavity geometry for 1 nC bunches shows that C-band (5.712 GHz) is the optimal frequency to realize C^3. The principal trade-offs are a reduced structure efficiency at lower frequency, but better beam dynamics for the 1 nC electron bunch train. C-band allows us to maintain a highly efficient structure, high gradient operation and excellent beam dynamics with proper damping and detuning of the cavities.

C^3 utilizes split-block fabrication to produce $\sim$ 1 meter structures with all cavities machined out of two or four copper slabs. The cavities are machined with modern CNC methods and the cavity surfaces require no post CNC machining, greatly reducing the production cost. Bonding of the two halves is needed, but the bonding is parallel to the direction of current flow and has an extremely small impact on the RF performance of the accelerating mode. Higher-order mode detuning can be incorporated by adjusting the cavity geometry of each cell during fabrication. This is already a standard procedure. Slot damping with lossy materials will suppress long range wakefields further.

These two ideas are the basis for a new, highly efficient generation of copper RF accelerators. We now turn to the question of how these features can be demonstrated to give a firm foundation for the C^3 design.

2.2 Optimization of the RF accelerating structure

The final accelerator structure for C^3 including wakefield damping and detuning will be fabricated and tested in the first year of the demonstration facility described in the next section. This meter scale structure will integrate all of the advanced concepts and meet all of the technical requirements for

2023 JINST 18 P09040

C^3, including operation at high gradient. However, many of these key concepts and design elements have already been demonstrated using current laboratory facilities, and we continue to advance the state of the art to increase the technical readiness of C^3.

High gradient operation of a distributed coupling accelerator at normal and cryogenic temperatures has already been demonstrated (including acceleration of beam) in multiple single and multi-cell structures [4, 5, 90, 91]. High gradient operation with low breakdown rate has been demonstrated at C-band [92]. A one-meter C^3 prototype was fabricated using the desired split-block technique and passed low power RF tests at cryogenic temperatures [93]. Slot damping features were incorporated into a prototype structure without reducing RF performance. Cryogenic RF properties were measured at C-band, demonstrating a reduction of a factor of more than 2.5 in RF surface resistance [94]. RF designs for cavity detuning and cavity damping to meet the requirements for a multi-TeV collider have been developed. Additional structures are now being produced and tested. Since testing does not necessarily require cryogenic operation, we expect that the structures can be quickly optimized.

Distributed coupling also allows one to optimize the phase advance between cells while adjusting for the cavity length. For the requirements imposed from short and long range wakefields, a cavity phase advance of 135° is optimal and allows us to increase the aperture to 3.55 mm while keeping the shunt impedance constant (120 MΩ/m) compared to the π-mode with an aperture of 2.62 mm. This approach provides a 300 MΩ/m shunt impedance for its planned mode of operation (beam aperture radius 3.55 mm). For comparison, NLC structures operated with a shunt impedance of up to 98 MΩ/m for the periodic cells (with a standing wave equivalent shunt impedance of 50 MΩ/m) [39], albeit with a larger aperture (beam aperture radius 3.75 mm). CLIC structures currently under consideration operate with a shunt impedance of 95.4 MΩ/m (with a standing wave equivalent shunt impedance of 39 MΩ/m) and a beam aperture radius 3.15–2.35 mm [40].

Combining all of these advances into a single mass-producible accelerating structure remains a high priority that must be completed early in the demonstration facility phase of the program. We plan that the complete damped and detuned accelerating structure design will be fabricated in the first year of the demonstration facility, allowing for engineering refinements of the structure. The accelerating structure can be fully tested outside of the cryomodule, allowing for multiple iterations during the operation of the demonstration facility if these are needed.

2.2.1 Accelerating structures for main linac and electron and positron source linacs

The implementation of new approaches to designing, building and operating a normal conducting accelerator structure has been key to the development of the technology for C^3. The discovery process began with an *ab initio* study of cavity shapes to maximize the on-axis accelerating field while minimizing probability of breakdown. After the first optimization, some suitable cavity shapes were proposed, however the optimized shapes had very small beam irises that precluded travelling-wave cavity coupling for the fundamental accelerating mode. As an alternative to on-axis coupling a distributed rf coupling scheme was proposed, implemented by parallel manifold rf waveguides providing side-coupling into each cavity with the proper rf phase and fraction of the inlet rf power. It was concluded that this relatively complex structure could be machined in two halves (or 4 quarters) by low-cost numerically-controlled milling machines. In addition to allowing for fabrication of the complex cavity shapes, this novel milling process results in ultra-high-vacuum (UHV) quality

2023 JINST 18 P09040

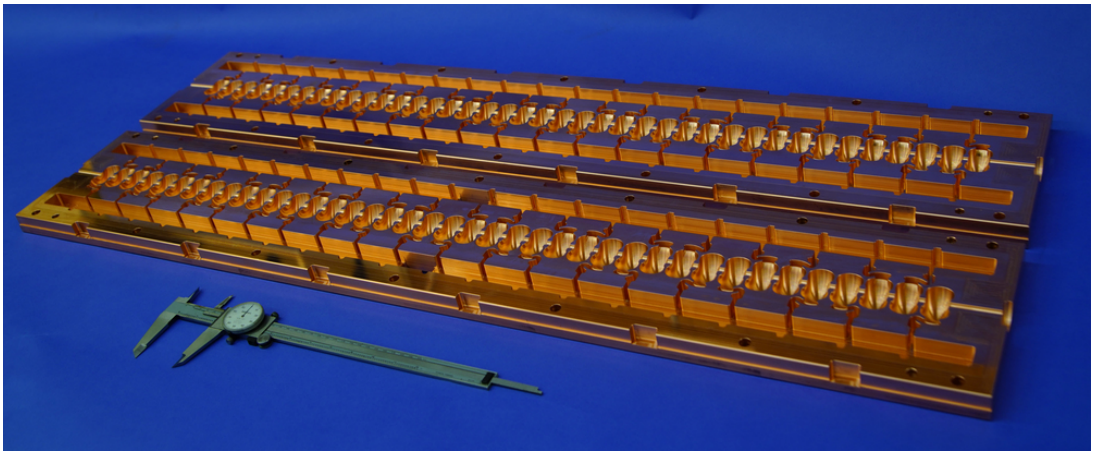

Figure 3. Both halves of the C^3 prototype structure prior to braze. The one meter structure consists of 40 cavities. A rf manifold that runs parallel to the structure feeds 20 cavities on each side. The structure operates at 5.712 GHz.

surfaces that need no further finishing apart from a standard copper surface etch. The final element of the proposed approach is operating the copper accelerator at a reduced temperature to increase the electrical conductivity of the material and improve the material strength and reduce probability of breakdown. The benefit of increasing electrical conductivity is in the reduction of the required rf power, as the rf power sources are a costly and complex part of the linac infrastructure. Increased conductivity also reduces thermal stresses in the material that result in cyclic fatigue of the material exposed to rf pulses, crystal growth, motion of dislocations and eventually in electrical breakdown. The onset of breakdown limits the achievable gradient for the accelerating structure and sets the practical gradient limit that the main linac can be operated at without degrading luminosity.

The C^3 structures will operate in a bath of LN_2 cooled to a cryogenic temperature of approximately ~ 80 K. The increased conductivity of copper at this temperature results in a shunt impedance of the optimized accelerator cavity of 300 MΩ/m, six times the effective shunt impedance of the Next Linear Collider (NLC) X-band accelerating structure.

The C^3 accelerating structure utilizes a copper standing wave distributed coupling rf structure. The first meter-scale prototype C^3 structure is shown in figure 3. The aperture of the cavity is determined by considering short-range and long-range wakefield effects for the nominal bunch charge of 1 nC. The baseline phase advance between cells is π. The frequency of operation for the main linac will be 5.712 GHz (C-band) in order to provide a high shunt impedance. For the electron source, positron capture linac and booster linacs into the damping ring, the operational frequency will be at S-band (2.856 GHz) to accommodate the longer electron and positron bunch length before compression. Prototype one meter accelerating structures have been fabricated and tested at high gradient and at cryogenic temperatures. A similar C-band accelerating structure was recently tested at Radiabeam and their room-temperature high gradient test setup is shown in figure 4.

The currently existing prototype accelerating structures are sufficiently advanced to determine the rf power requirements, thermal loading, geometrical constraints and suitability of manufacturing techniques. Still, significant optimization of the accelerating structure within these limits is possible and will be the focus of early stage R&D in this demonstration plan. Remaining within these limits

2023 JINST 18 P09040

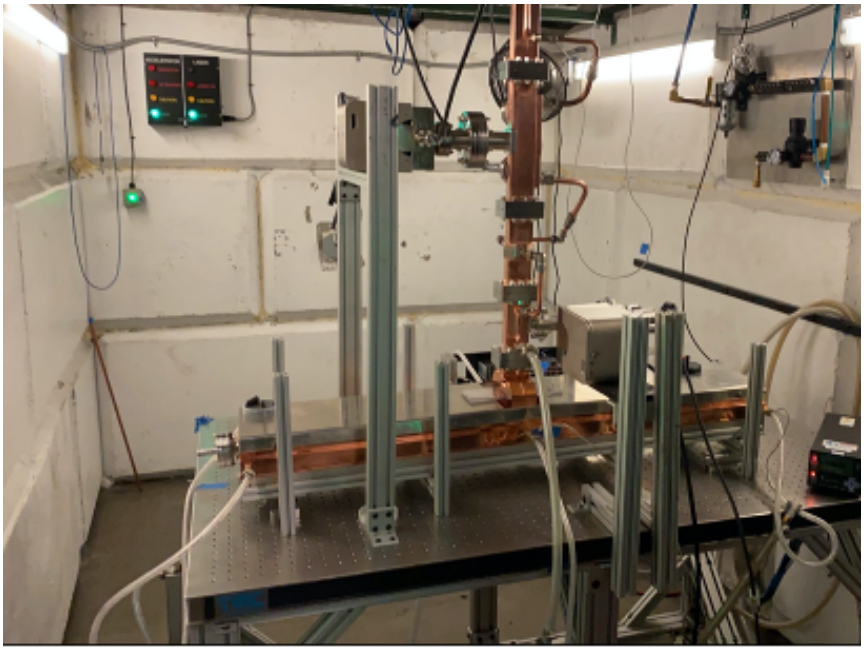

Figure 4. The C^3 prototype structure in test at Radiabeam. Both room temperature and cryogenic tests will be conducted as part of the C^3 Demonstration R&D Plan to quantify improvements to the structure performance as we incorporate damping and detuning in the design.

will allow improvements to the accelerator structure without requiring a redesign of the cryomodule internals. These improvements to the accelerating structure are in large part enabled by the rf design of the distributed coupling topology which allows for fabrication of the structure in halves, thereby allowing for simplified incorporation of rf distribution and damping.

Accelerator structure R&D topics.

- *Manufacturing* — Minimizing part count, minimizing raw material, simplifying assembly and automating quality control and tuning.
- *Bonding Techniques* — Optimization of brazing with laser-cut shims, and exploration of alternative low temperature techniques with electron beam welding or diffusion bonding to increase throughput.
- *RF Design* — Optimization of rf phase advance to $3\pi/4$ phase advance per cell, reduced cell length and proper power and phase rf manifold design for distributed coupling.
- *Damping* — Advanced modeling and engineering are required to finalize the design of wakefield damping features in the cavity. Material loss and performance in UHV and high field environment must also be confirmed. Leading material candidates are: NiCr, FeCrAl with a special technology of coat, SiGraSiC-group composits, and doped SiC.
- *Thermomechanical Analysis* — Vibration, alignment, tolerancing, and thermal analysis of accelerating structure.

2023 JINST 18 P09040

- *Enhancement of heat transfer to LN_2* — Optimization of the accelerator structure surface profile to minimize N_2 gas bubble trapping under the accelerator structure; exploring surface treatment for example, special texturing and coatings that enhance nucleate boiling heat transfer; surface passivation techniques that prevent surface oxidation (oxidation is known to reduce nucleate boiling heat transfer over time and so should be prevented).

2.2.2 Accelerator structure for injector linac

In order to efficiently handle high bunch charges and minimize wakefields for electron and positron injection, a large beam aperture is typically needed. Leveraging the design language from the development of the C^3 main structure, a similar structure at S-band was designed to incorporate distributed coupling and wide aperture re-entrant style cavities. This design allows for each cavity to be optimized for shunt impedance, allowing a single 1-m structure to provide an accelerating gradient of up to 85 MV/m with 35 MW of rf power when cooled to ~ 80 K as with the C^3 main structure. Current prototypes are being assembled and tuned, with plans in place to conduct high power and acceleration tests at both room temperature and ~ 80 K in the near future. The next revision of this design will also take into account the dimensions of the C^3 cryomodule design, so that the same cryomodule could house either C^3 main structures or these S-band injector linacs.

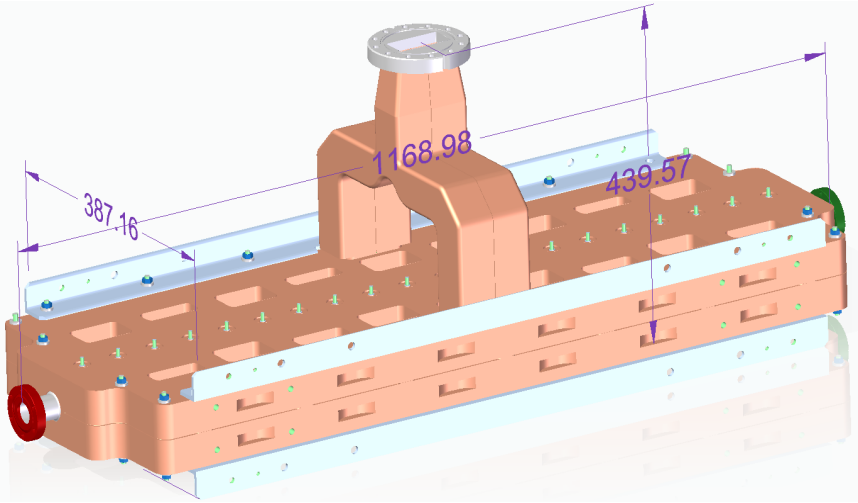

Figure 5. The prototype design for S-Band injector linac. Two structures are currently being assembled, and both room temperature and cryogenic tests will be conducted to validate performance. Dimensions are in mm.

2.3 RF distribution

Any concept for a distributed feeding network is required to simultaneously provide power and the appropriate phase advance for each cell. In this case, the cells are identical and require equal power and a constant phase advance. For a typical electron linac with a particle moving at nearly the speed of light, the phase advance per cell is $2\pi P/\lambda$; where P is the periodic separation between cells and λ is the free space wavelength. With the exception of a dielectric-free coaxial line, this phase advance cannot be provided by any form of wave guiding structure, which always have a guided wavelength $\lambda_g > \lambda$. Alternatively, one can use waveguides oriented so that the center E-plane is

2023 JINST 18 P09040

the same as the E-plane of the accelerator cell. [42] Because the guided wavelength does not match the free-space wavelength, one can imagine solutions where the distribution waveguide is bent like a serpent to achieve the appropriate phase advance. This is valid, but one can use more than a single manifold. A natural interval in spacing for tapping into the RF waveguide manifold with power couplers, as shown below, is every $m\lambda_g/2$. Here, λ_g is the guided wavelength within the manifold and m is an integer. Therefore, for a structure with a phase advance/cavity of $2\pi/n$, one can use n manifolds where each one of them is being tapped every λ_g. Hence the phase advance is also an optimization parameter.

A π phase advance per cavity is a special case that simplifies the design of the system. In this case, $n = 2$ and only two manifolds are needed. Initial distributed coupling structures shown in figure 3 have this mode of operation, which is close to being optimal. For the large-scale optimization of a collider structure with small beam apertures, a phase advance of $3\pi/4$ has the same shunt impedance, see figure 6, but a significantly larger iris aperture (radius of 3.55 mm vs. 2.62 mm). An RF distribution manifold will therefore require design for this phase advance as shown in, figure 7. As described, each segment of the distributed-coupling accelerator structure can be manufactured from two blocks as shown in figure 3 or four blocks. The structure is designed so there are no currents crossing the mid-plane along the long dimension. This reduces the complexity of manufacturing the structure and provides logical places for both the cooling manifolds and the tuning holes. The manifold consists of a set of cascaded T-junctions with power going through the tap-off ports. The cavity coupling port is designed to give a matched port when the cavity is loaded with the design current.

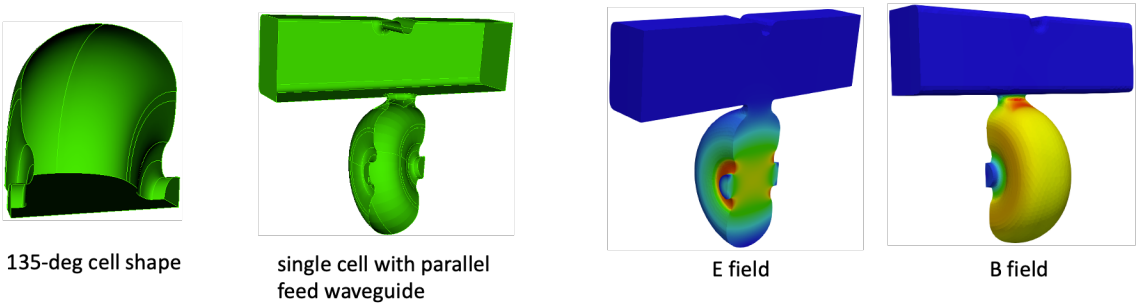

Figure 6. Cavity and periodic manifold design for $3\pi/4$ phase advance.

2.4 Wakefields

Wakefields and the resulting emittance degradation are of significant concern for any practical collider design. A complete wakefield analysis requires advanced beam dynamics simulations that account for both short-range and long-range effects. They must include operational machine tolerances, the design and optimization of wakefield damping, and cell detuning to mitigate long-range wakes. While a complete analysis and design is beyond the scope of this work, an initial effort to ascertain the validity of this structure was undertaken using the performance characteristics of existing collider designs.

The proposed C^3 beam format consists of trains of the electron bunches recurring at 120 Hz. Each train will have 133 bunches with the bunch charges of 1 nC separated by 5 ns for C^3-250, and by 3 ns for C^3-550. This short bunch separation requires sophisticated wakefield control to prevent emittance growth. Besides, the small diameter of the iris aperture of $a/\lambda = 0.065$ has the potential

2023 JINST 18 P09040

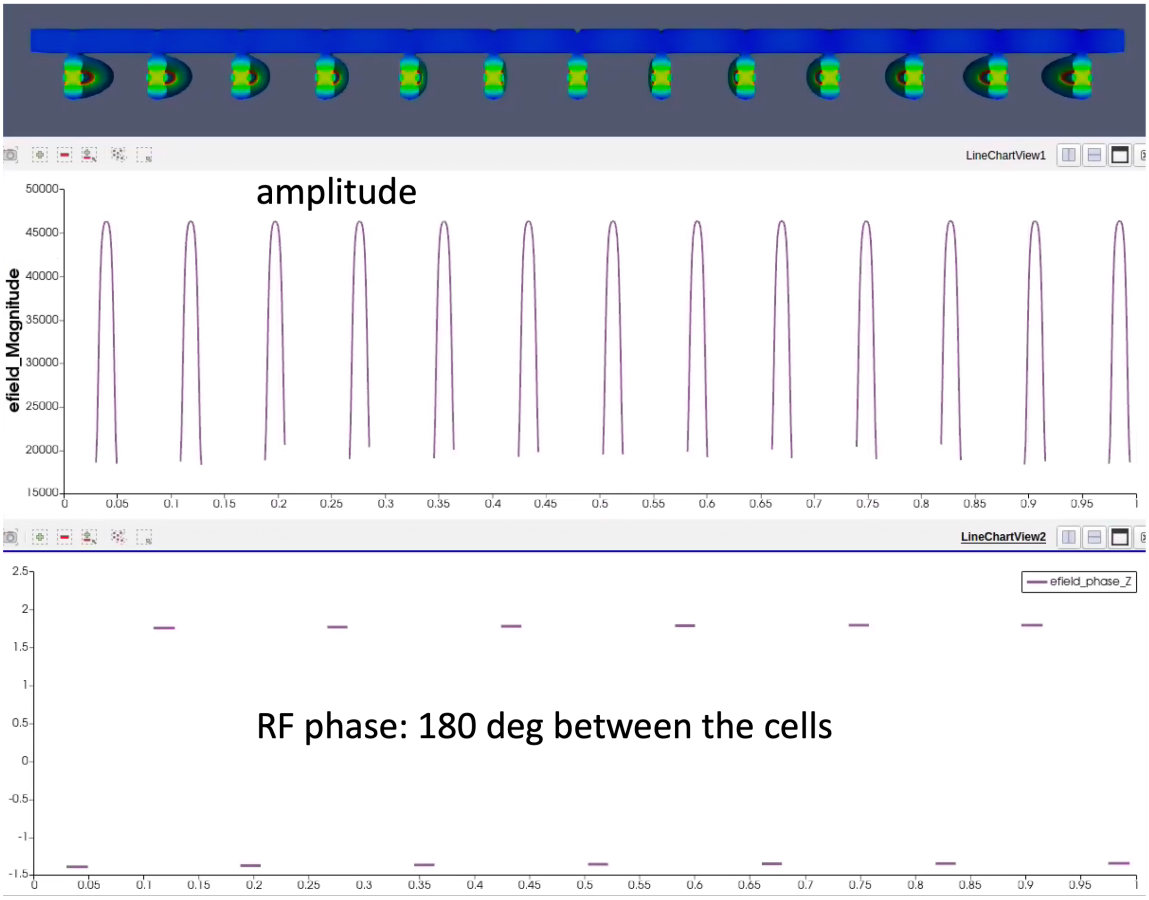

Figure 7. Manifold for RF distribution for the proposed parallel feed waveguide $3\pi/4$ C-band structure.

to result in significant short range wake effects. The emittance growth in the structure was analyzed for various beam parameters by varying the offset in phase for longitudinal wake suppression and varying the bunch length for transverse wake suppression. The goal of this simulation was to achieve a residual energy spread in the range of $\sigma_{\delta 0} = 2\text{–}5 \times 10^{-3}$ and a maximum of 1% correlated energy spread for Balakin-Novokhatski-Smirnov (BNS) damping, which was analyzed with transport simulations in the main linac [41].

Ongoing R&D for the structure development is focused on the design of the structure's damping and detuning to mitigate the effects of long range wakefields. The kick factor must be suppressed below 1 V/pC/mm/m to provide stable transport of the electron and positron beams. Detuning of higher order modes is achieved by modifying the geometry of each cavity while maintaining constant frequency of the fundamental mode. The frequencies of higher order modes vary as a result of geometrical changes. Simulations have shown that 4σ Gaussian detuning with a $\Delta f/f_c$ of 6% is sufficient to suppress the longitudinal wake for the first subsequent bunch for the first dipole band [41]. Detuned cavity designs exist already and they can cover the necessary range in frequency ($\Delta f/f_c = 6\%$). For longer range damping we are designing a structure with the use of longitudinal damping slots in quadrature that meets the required reduction in quality factor for higher order modes.

2023 JINST 18 P09040

2.4.1 Long-range Wakefield

Damping of the long-range wakefield was the subject of extensive investigations for collider designs such as NLC and CLIC. Both of these accelerator designs have incorporated cell-to-cell detuning and damping for wakefield suppression. Detuning works by preventing the coherent addition of dipole modes along the length of the structure. In order to achieve detuning, small modifications must be designed and incorporated into each cell of the structure. The modifications require simulation and design with high-performance computing tools that have been developed for linear collider structure design. The efficacy of detuning is limited by the eventual recoherence of the wakefield modes in the structure. Therefore, broadband damping must be added to suppress the wakefields. In order to symmetrically suppress both orientations of the dipole mode, structures have been designed with four apertures in each cell that couple either to individually damped waveguides containing an absorbing material (SiC) or to common manifolds that transport the power away from the structure to a common load.

Understandably, in the actual structure for the main linac presented in this design, these two well-known means of wakefield suppression will need to be incorporated in two ways. First, by detuning the dipole frequency in a Gaussian density distribution, the wakefield can be dramatically suppressed in a short distance, e.g. at the second bunch of the bunch train. Second, with damping to suppress the wakefield at a longer distance from recoherence of the detuned modes, ideally through the existing manifold and an additional one for the second orientation of the dipole mode.

The most immediate concern for long-range wakefields are the dipole modes. The dominant contribution to the long-range dipole wakefield is from the first 2 to 3 dipole passbands of the structure. The contribution of each mode is quantified by the kick factor determined by the structure's geometry. As a function of distance, the long-range dipole wakefield is calculated as the sum of the sinusoidal spatial oscillations with wavenumbers ωn/c, scaled by the kick factors. The dipole wakefield was calculated for a 20-cell C-band structure. The 20 cells are identical and there is no de-tuning incorporated (see figure 1). While the wakefield of such a structure does not represent the final design for a linear collider, the calculation presented here provides a realistic peak value for comparison with other designs.

Figure 8 shows the dipole wakefield for a uniform 20-cell C-band structure. Each cell is 1/3 of a wavelength and the total structure length is 351 mm. A Qdamp of 1000 was used for all the dipole modes. The peak value of the transverse wakefield at the origin is about 50 V/pC/mm/m. This value is about half that of the X-band structure proposed for the NLC. The bunch spacing in consideration is 19 periods of the C-band wavelength, which is about 1 m. Based on the X-band structure studies for the NLC, about 10% detuning of the dipole modes would be needed to minimize the wakefield at the first subsequent bunch by a factor of > 50. The exact value will depend on the number of modes used for the detuning.

In figure 9 we see that for the first dipole band, a four-sigma Gaussian detuning does provide suppression for the first subsequent bunch located at $s = 1$ m. With the decoherence optimized for one meter, a recoherence of the wakefield is observed by 75 m. This distance is close to the length of the bunch train. Simulations shown in figure 10 introduce a damping mechanism that reduces the quality factor for the dipole modes to 1000, completely suppressing the recoherence. This damping mechanism is not yet designed. One possible solution is utilizing the parallel feeding waveguide, figure 4 and figure 5, for the C-band design which can naturally provide manifold damping for the dipole modes. Additional damping schemes can be added to achieve the needed damping for both x-y polarizations.

2023 JINST 18 P09040

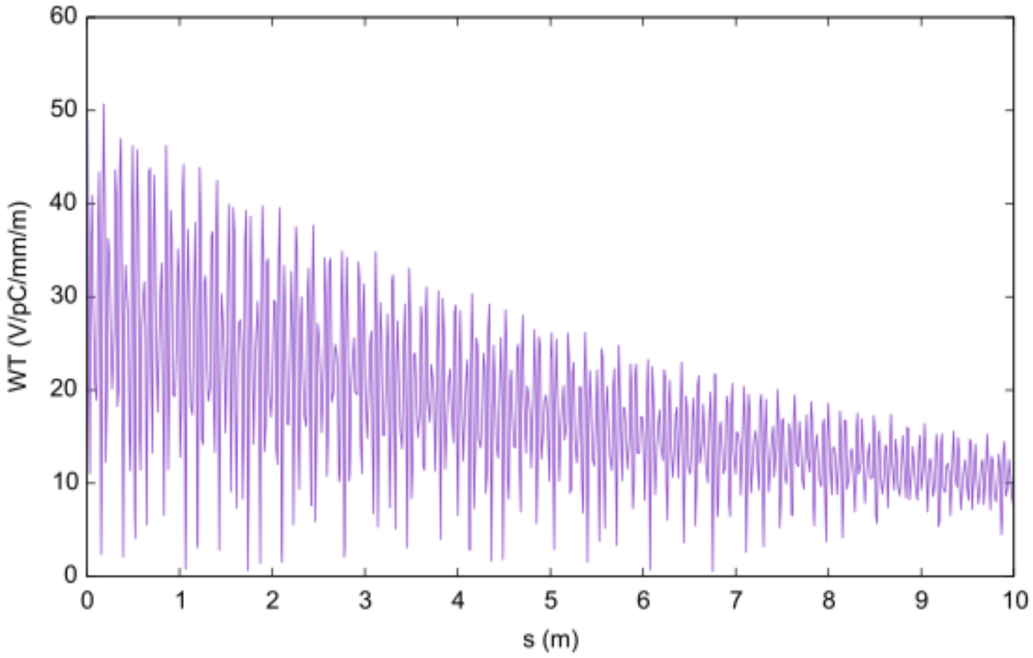

Figure 8. Long-range transverse dipole wakefield envelope for the uniform 20-cell C-band structure shown in figure 1.

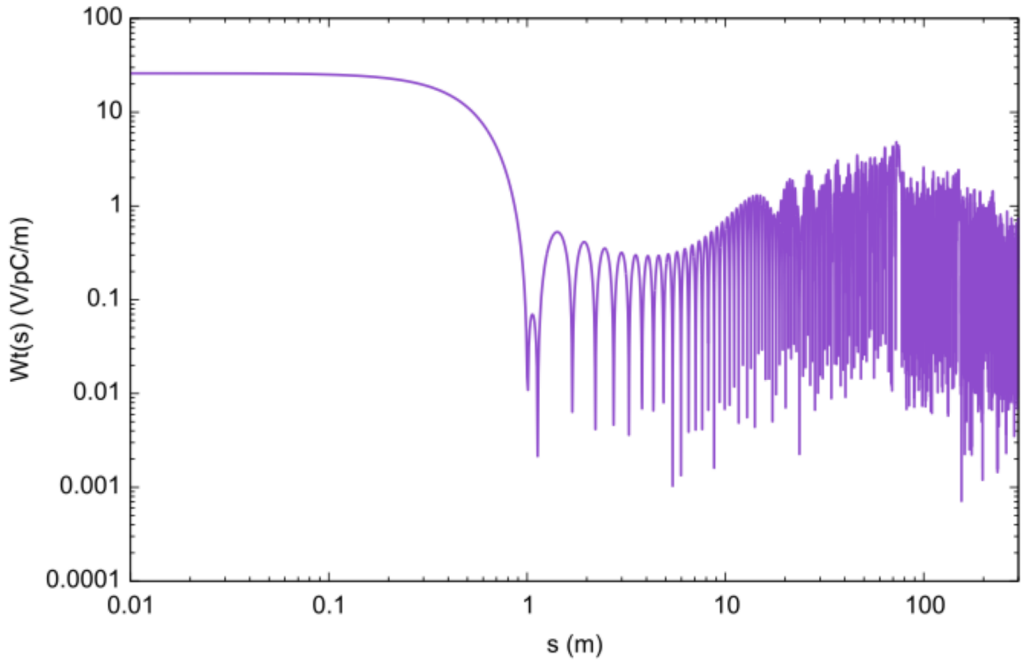

Figure 9. Long-range wakefield calculation for the first dipole band with cell detuning incorporated. In this simulation a four-sigma detuning is utilized over 80 cells of structure ($\sim$ 2 m), centered at a frequency of 9.5 GHz with a $\Delta f / f_c$ of 5.6%. These simulations include ohmic losses from the copper walls of the structure.

2023 JINST 18 P09040

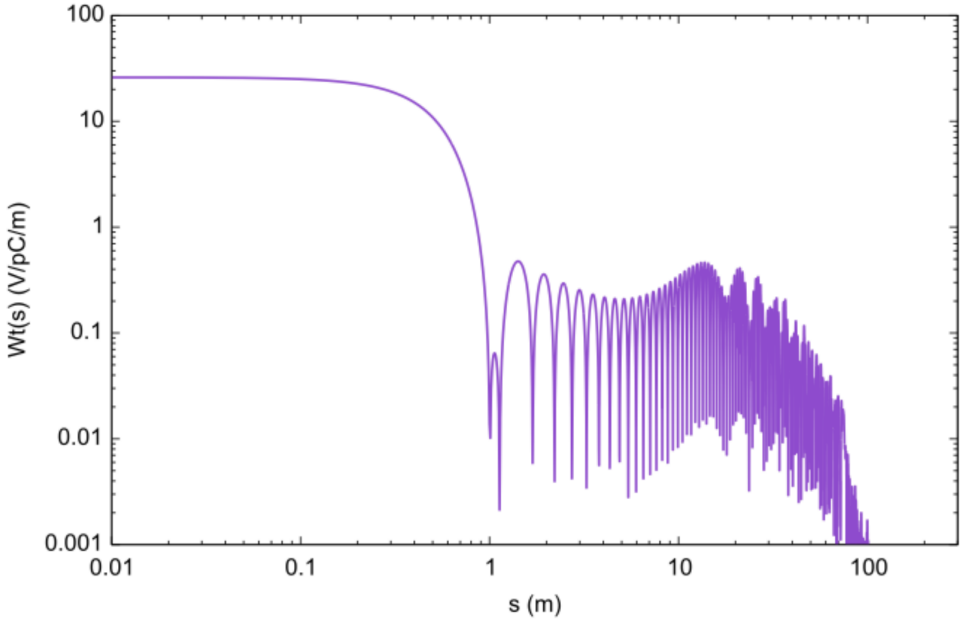

Figure 10. Long-range wakefield calculation for the first dipole band with cell detuning and an artificial damping factor incorporated. The damping reduces the qualify factor of the dipole modes to 1000. The detuning parameters are the same as the simulations in figure 9.

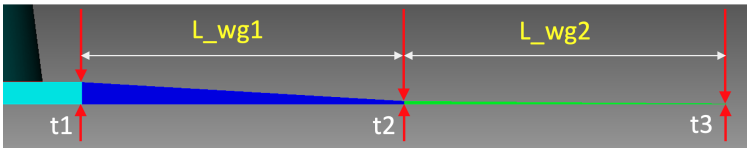

Figure 11. Slot geometry for damping simulations. Slot walls assigned a conductivity of 10^6 S/m which is equivalent to NiChrome at 80 K.

2.4.2 Damping features and materials

To reduce the quality factor for higher order modes in the accelerating structure a significant amount of damping is required. In addition, the damping must occur in a structure operating at low temperature where the conductivity of materials may be significantly different than traditional use cases at room temperature. Preliminary simulations indicated that damping slots [43] in quadrature that cut through the cell iris and coupling slots provides sufficient damping of higher order modes up to 40 GHz [44, 45]. The damping slot geometry is flexible and the aperture, length and taper should be optimized for the absorption of power across the full spectrum of modes. Simulations of a two step, figure 11, showing suppression of the kick factor are shown in figure 12. The walls of the damping slot are assumed to be coated with the lossy metallic conductor NiChrome which has a relatively poor conductivity of 10^6 S/m at 80 K as confirmed by rf measurements and can be deposited either through sputtering or chemical deposition.

2023 JINST 18 P09040

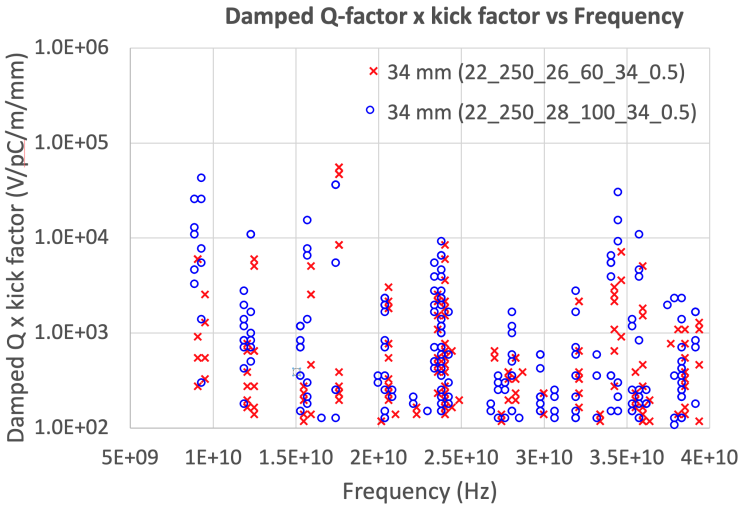

Figure 12. Kick factor multiplied by Q showing a strong suppression of long range wakefield effects.

2.4.3 Alignment and vibration tolerances

Alignment and vibration tolerances form one of the most critical set of parameters that must be achieved for C^3. The constraints on component alignment and vibrations, table 2, are due to the small structure aperture and extremely small vertical emittance. The C^3 main linac will utilize beam based feedback and alignment in order to achieve the design luminosity. It is envisioned that this will include 1-1 steering, Dispersion Free Steering (DFS) and wakefield bumps. This relaxes the initial alignment tolerances from 10s of nanometers to 10s of microns or larger for longer wavelength misalignmets [46], as shown in figure 13.

Motion of components and the beam on a shot-to-shot basis that is too fast for feedback systems to compensate will place a vibration tolerance on components and injection alignment tolerance for the beam. The sensitivity to the random motion of components for structures, quads and injection into the main linac is shown in figure 14

3 C^3 demonstration R&D

To complete the TDR for the accelerator that we describe here, we will need a full demonstration of the C^3 Main Linac technology on the GeV scale. This demonstration can be done in parallel with the preparation of the TDR. The outstanding technical achievements of the ILC, CLIC and NLC collaborations are central to the rapid realization of the C^3 proposal. Many of the subsystems for the accelerator complex are interchangeable between linear collider concepts with manageable modifications to account for variations in pulse format and beam energy. Because these subsystems are already mature, the C^3 demonstration facility can focus on the specific set of technical milestones associated with the C^3 concept itself:

- Development of a fully engineered and operational cryomodule including linac supports, alignment, magnets, BPMs, RF/electrical feedthroughs, liquid and gaseous nitrogen flow, and safety features.

2023 JINST 18 P09040

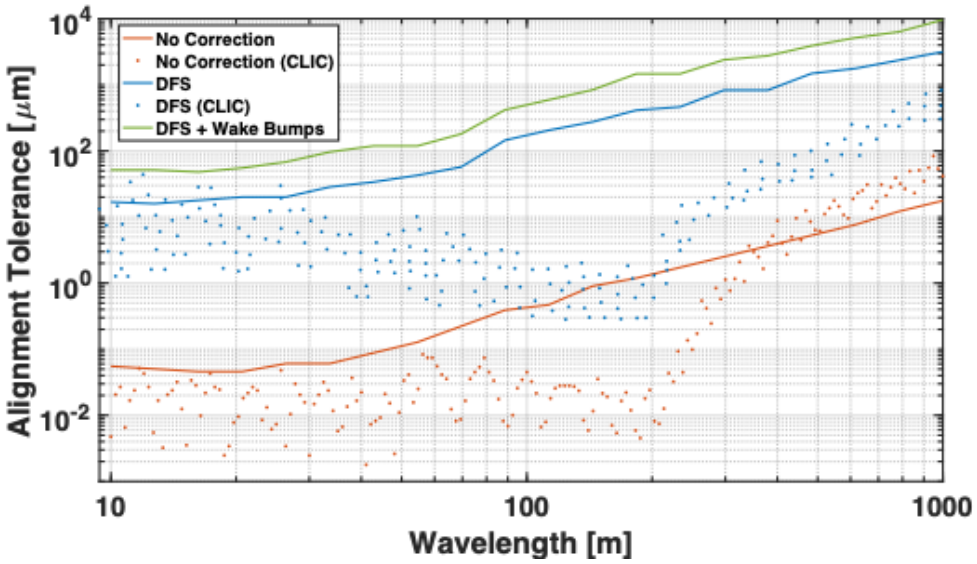

Figure 13. Tolerances vs. misalignment wavelength for various levels of beam based alignment. The dots are from CLIC studies and are shown for comparison.

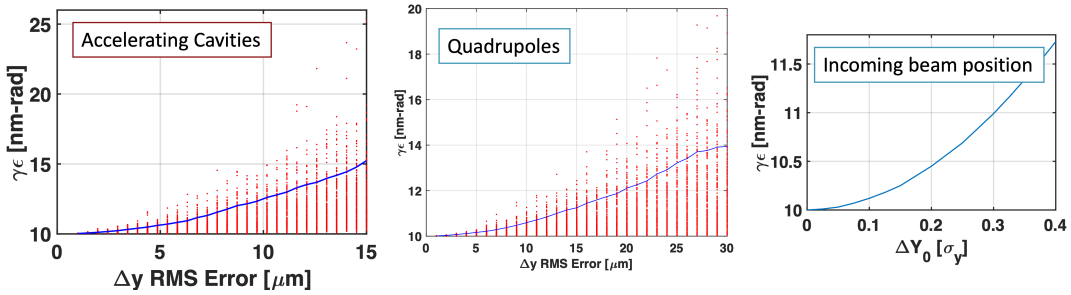

Figure 14. Sensitivity to component vibrations.

- Operation of the cryomodule under the full thermal load of the Main Linac and maximum liquid nitrogen flow velocity over the accelerators in the cryomodule, demonstrating an acceptable level of vibrations.

- Operation with a multi-bunch photo-injector to induce wake fields, using 8 high charge bunches and a tunable-delay witness bunch.

- Achievement of 120 MeV/m accelerating gradient in single bunch mode for an energy gain of 1 GeV in a single cryomodule, including tests at higher gradients to establish breakdown rates.

- Acceleration and wakefield effect measurements with a fully damped-detuned structure.

- Development, in partnership with industry, of the baseline C-band RF source unit that will be installed with the Main Linac. The RF source unit will be modified from existing industrial product lines.

2023 JINST 18 P09040

We propose a staged R&D plan that will culminate in the construction of a 3 cryomodule linac with the cryomodules being pre-production prototypes. This linac would be fed by an S-band rf photo-injector, a booster linac and a magnetic bunch compressor. The injector would utilize accelerator technology that would be suitable for the electron source and positron capture linac. The linac would feed an energy spectrometer for direct gradient measurements and then send the beam to a dump. This linac and electron source technology will serve as direct prototypes for FELs and other instruments requiring a high brightness, high gradient, compact linac. The full demonstration linac is shown in figure 15. The target tolerances for the injector and cryomodule are listed in table 2. A more detailed view of a single cryomodule is shown in figure 16.

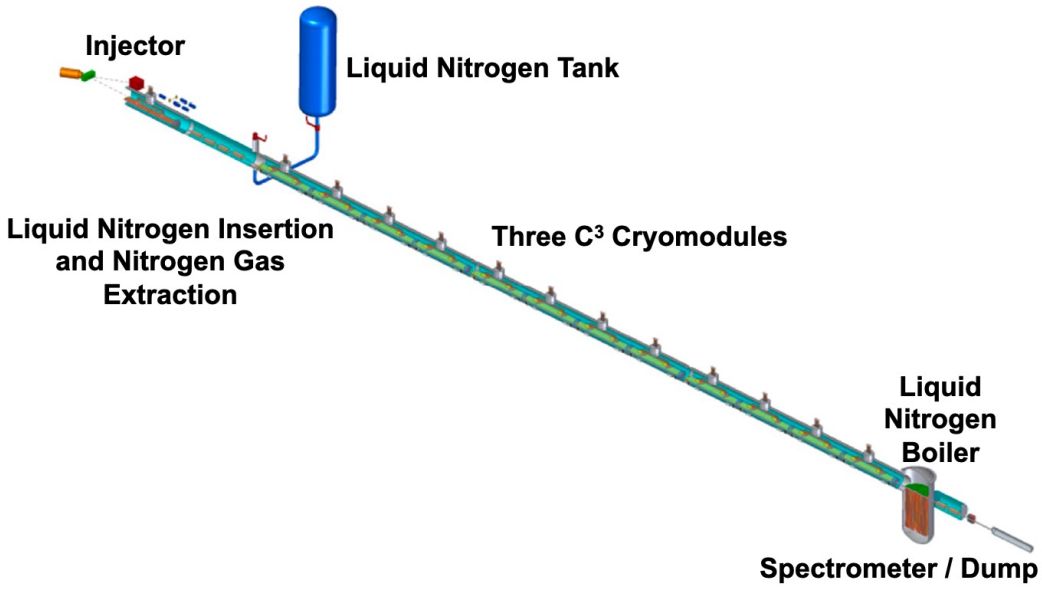

Figure 15. Schematic of the full 3 cryomodule C^3 demonstrator capable of achieving all of the technical milestones for the R&D plan. The full length of the layout it ~ 50 m.

The injector for the demonstrator linac will consist of an rf photo-injector with a removable CsTe cathode [49] or another cathode material capable of producing suitable electron bunches. The goal will be to extract up to 133 nC of charge over 700 ns from the photo-injector to match the beam loading of the C^3 main linac. The individual bunch charge will vary depending on the beam test that is being conducted. Beam dynamics simulations of the injector and demonstrator linac will determine the target bunch charge and bunch spacing. The photo-injector will operate at S-band (a sub-harmonic of the C-band accelerator frequency). The photo-injector will produce 3–5 MeV electron bunches. This will be followed by matching optics to inject the beam into two one-meter long S-band accelerating structures operating at cryogenic temperatures. These linacs will operate at 50 MeV/m and will have a large transverse aperture to minimize any short- or long-range wakefields. The S-band section will bring the beam energy to 100 MeV. A magnetic chicane will be used to compress the electron bunches prior to injection into the first C-band cryomodule.

2023 JINST 18 P09040

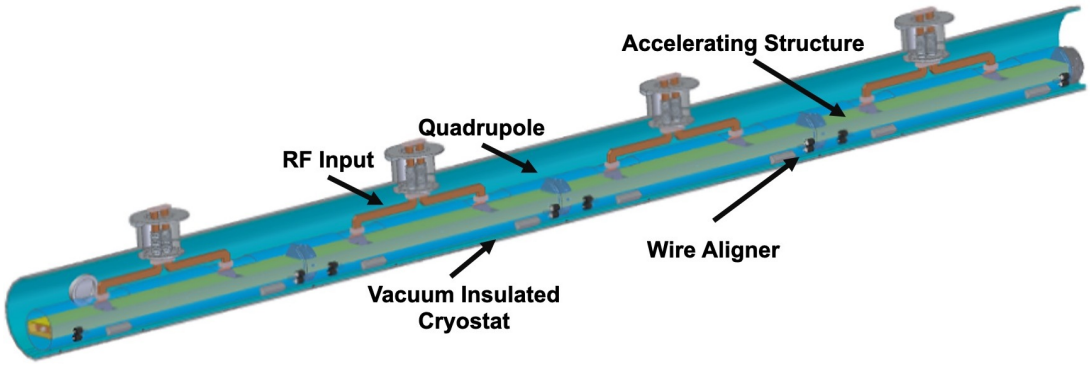

Figure 16. Rendering of the 9 m C^3 cryomodule with 8 one meter accelerating structures, 4 two meter support rafts, 4 permanent magnetic quadrupoles and integrated beam position monitors.

3.1 Objectives & timeline

The objective of the C^3 Demonstration R&D Plan is aimed at mitigating C^3 technical, schedule, and cost risks by achieving the following Technical Milestones and the Critical Parameters in table 2:

- High-gradient (≥155 MeV/m) test with gradient margins of a damped and detuned C^3 accelerating structures at S-band and C-band
- Testing of the cryomodule at gradients required for C^3-550 (goal is to reach ≥ 155 MeV/m for margin)
- Demonstration of a fully engineered cryomodule with full beam loading in at least one cryomodule
- Demonstration of full C^3 LN_2 and vapor flow in 3 cryomodules as well as verification of vibrations and alignment stability.
- Experimental verification of the tolerances and specifications for production of the main linac cryomodules, including assembly procedures.
- Demonstration of a viable rotation and cooling system for a positron production target

The timeline for progressing with C^3 technology development will be governed by practical limitations on both the technical progress and resource availability. Here we present the technically limited timeline for the Demonstrator R&D Plan. The detailed breakdown is shown in figure 17.

Stage 0. At present, fundamental rf accelerator R&D that is relevant to C^3 is ongoing with the investigation of high-gradient accelerating structures, rf design, rf components for power distribution and compression, frequency and temperature scaling, materials, manufacturing techniques, wakefield suppression, novel rf source concepts, and experimental prototypes at the meter scale. This fundamental R&D is directly impacting the development of small-scale and compact accelerators for industrial, security and medical applications ranging from 10–100 MeV. These advances are also impacting larger scale facilities, for example with the adoption of new concepts for pulse compression and transverse deflectors. This technology is also being adopted for both the rf gun and linac for compact x-ray and FEL sources.

2023 JINST 18 P09040

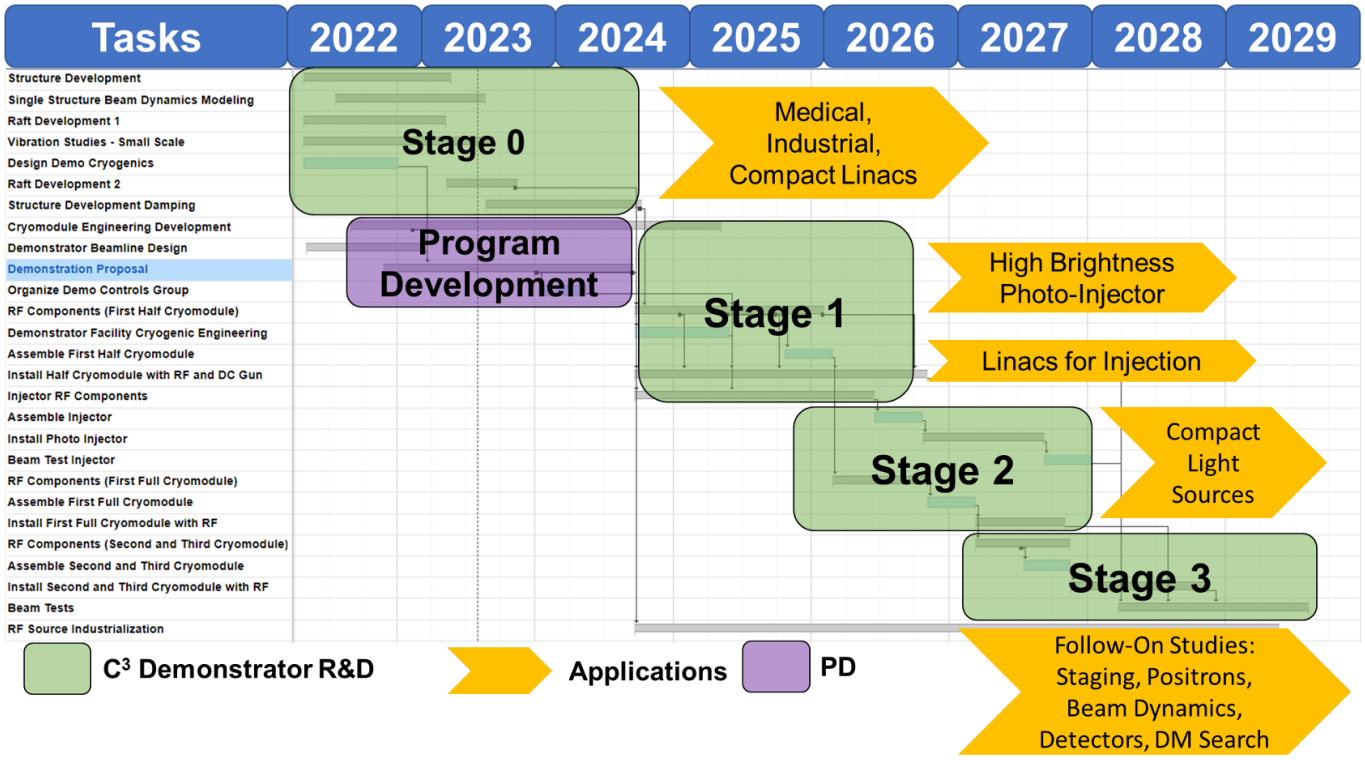

Figure 17. C^3 Demonstration R&D Plan timeline. The timeline is undertaken in four stages. Stage 0 consists of ongoing fundamental R&D for structure design, manufacture and test. Including operation at high gradient, damping and detuning designs, vibrations and beam test. Stage 1 is the preparatory phase for preliminary engineering studies and submission of a full proposal. Stage 2 delivers the first cryomodule, the injector and beam tests at the full C^3 accelerating gradient. Stage 3 completes two additional cryomodules and completes beam tests. Many applications will be enable by this technology development plan and the rough timeline for those applications is also highlighted.

Table 2. Critical parameters.

Accelerating Structure	
Gradient (MeV/m)	70/120
Flat Top (ns)	700/250
Shunt Impedance (MΩ/m)	300
Breakdown Rate (/pulse/m)	3×10^{-7}
Beam Loading (%)	45
Alignment & Vibrations	
Main Linac Components (μm)	10
Beam Delivery System Components (μm)	10
Vertical Stabilization Linac Quad (nm > 1 Hz)	1.5

Through the Snowmass process we are actively exploring how these innovations in rf accelerator technology impact the design of C^3 facilities that scale from Higgs factory to a few TeV. This has allowed us to identify the key parameters and milestones for advancing the C^3 concept.

Stage 1 for the C^3 Demonstration R&D Plan will serve to advance the development of C^3 technology to a level of engineered maturity to form the basis for a demonstrator proposal. In particular, we will focus on the engineering of the cryomodules that would be tested as part of the demonstrator. This will include a damped-detuned accelerating structure, prototype support rafts with alignment and vibration suppression, and full consideration of the cryogenics design of the cryomodule. This will also include the design of the injector and C^3 demonstrator beamline design with start-to-end simulations including space-charge and wakefield effects. Beam tests will be performed in structures operating at cryogenic temperature to test full beam loading. In addition to providing the technical information needed to produce a full demonstrator proposal, Stage 1 activities will directly impact applications requiring compact accelerators. The injector design could also be utilized for applications targeting very high charge electron bunch sources (for examples as an upgrade to the EIC injector [93]) or the high-brightness rf photo-injector design could be utilized for a an upgrade to LCLS-I to produce very high energy soft x-ray pulses [50]. In particular, the distributed-coupling rf linac technology would also impact the realization of medium energy electron beam injectors as it provides for a resilient design against failures in the rf subsystems, i.e., klystrons. A demonstration S-band prototype accelerator structure for electron injectors is currently under construction at SLAC to demonstrate the attainable gradient, optimized beam aperture and operational reliability [93].

Stage 2 of the C^3 Demonstration R&D Plan will focus on the production and testing of the first cryomodule. The first engineered design for a full cryomodule will be tested initially with high power rf. The system will be operated at cryogenic temperatures. The gradients that are achieved would accelerate a beam to by 1 GeV in 9 m. Captured dark current would allow for confirmation of this energy gain and gradient. In parallel we will build and commission the electron source for the C^3 demonstrator. This will consist of a high-brightness rf photo-injector and two meters of S-band linac that can support high charge. This linac would be adopted in the electron and positron sources for C^3 up until the damping ring. After commissioning the injector, the photo-emitted beam would

2023 JINST 18 P09040

be compressed and transported into the first cryomodule and the first beam tests would commence. This would be a major milestone for C^3 and provide sufficient experimental data to compile a CDR, but also deliver a high-gradient accelerator technology that could be mass produced and used for compact FELs, XFELs, compact gamma ray sources, or a beam driver for PWFA. Stage 2 of the C^3 Demonstration R&D Plan is anticipated to take 3 years and concludes with the transport of photo-electrons through the first cryomodule.

Stage 3 of the C^3 Demonstration R&D Plan includes updates to the engineering design of the cryomodules, production of the second and third cryomodule and their installation. The LN_2 boiler would also be installed to allow for full thermal and vibration tests. After the installation of each cryomodule, beam tests would be performed with increasing beam current to test full beam loading. Lower charge and lower emittance beams would be used to investigate emittance growth. Stage 3 would be completed with the operation of the final cryomodule with beam at the C^3-550 gradient. Sufficient information would be produced mitigating C^3 technical, schedule, and cost risks required to proceed with a TDR. After Stage 3, the C^3 demonstrator could be utilized for a wide variety of R&D related to technological improvements for C^3 , related HEP R&D or other applications such as a compact FEL.

Completion of the C^3 Demonstration R&D Plan will allow us to achieve:

- Demonstration of feasibility and first optimization of the C^3 linac technology
- Design and optimization of the linear collider accelerator complex based on C^3 technology
- Confirm the suitability of the C^3 beam parameters for the physics reach and detector performance
- Preparation for a Conceptual Design Report (CDR)
- Preparation for follow-on technology development and industrialization

After completion of the demonstration milestones for C^3 , this facility would continue on with a high impact R&D program. It would provide opportunities to further advance the state of the art for C^3 upgrades (improvement of RF sources, testing with different bunch parameters and pulse formats, etc.). The demonstration accelerator would also provide a source or injector to enable R&D opportunities for other advanced accelerator concepts (such as gamma-gamma colliders, plasma wakefield acceleration, structure wakefield acceleration, etc.). These alternate concepts could also include C^3 technology in their eventual implementation. The facility would also carry out research on related accelerator R&D (FELs, beam dynamics, extreme bunch compression, etc.), including the possibility of staging multiple cryomodules to achieve higher energy.

3.1.1 Cryomodule cryogenics

The accelerating structure operates immersed in a liquid bath of LN_2 at $\sim$ 80 K. The thermal load of the accelerator is cooled by the boiling of liquid nitrogen. The cryomodule transports both the liquid and gaseous nitrogen in the same vacuum jacketed enclosure that houses the accelerator. The accelerator is in cryomodules that house 4 rafts; each raft supports 2 accelerator structures, a permanent magnet quadrupole, and beam position monitors (BPM). A rendering of the

C^3 cryomodule is shown in figure 16. The improvement in Cu conductivity at ~ 80 K improves the accelerator efficiency by a factor of 2.5–2.7× to more than recover the capital and operating expenses of the refrigeration plants. For the C^3 collider it is envisioned that the main linac sectors consist of 10 cryomodules, and super-sectors consist of 10 sectors.[1] A super-sector is supported by a single entry and exit point for liquid and gaseous nitrogen. It is anticipated that there will be either 2 or 3 super-sectors per main linac for C^3 .

The cryomodule is a vacuum insulated tube with an inner radius of 30 cm. The accelerator components are under slowly flowing LN_2 at a pressure of ~ 1.1 bar, with the LN_2 ~ 25 cm above the cryostat low point. The LN_2 is introduced at the super-sector boundaries or the ends, and flows in both directions (one if at an end) for at most 500 m. Gaseous nitrogen counter-flows, is removed at the boundaries or ends, is re-liquified, and then re-injected. The LN_2 for one direction of flow enters at 7.2 l/s, and flows at a velocity (at the entry) of 0.06 m/s (0.2 km/hr). The counterflow gas flow has an area equivalent to a 23 cm radius pipe, and has a pressure drop over the full length of ≤ 10 mbar.

The LN_2 flow is driven by gravity. For the C^3 collider, the spans between super-sectors are laser straight, the mid-span is normal to the earth radius there, and thus the LN_2 is deeper at the center of a super-sector by ~ 7 cm. The beam will be bent in the vertical plane at the super-sector boundary by ~ 80 micro-radians to go into the next super-sector. For a 100 GeV beam, this requires a dipole with a kick of 0.05 T-m. For C^3-250 and C^3-550, the power dissipated in one accelerator section is 2500 W, or 0.4 W/cm^2. This thermal load is constant because of the reduced flat top of the rf pulse. With this thermal load, the accelerator will operate in the nucleate boiling regime, and the expected temperature rise is ~ 2 K. The temperature rise in the copper block in a 1D approximation is 0.6 K.

The open channel ("river") of LN_2 flow must be driven by a pressure head, which comes from a liquid depth difference. The various features providing liquid flow area changes, like vertical waveguides and cryomodule interconnects, result in a resistance to liquid flow and could potentially create a liquid flow problem due to a large pressure head required. This will be carefully evaluated to provide the assured margin (through the cryomodule diameter) as the design progresses.

Very early in the conceptual design phase, it is important to consider failure modes and the potential impact on design features. One of those is loss of insulating vacuum, which is not unusual and often results from a leaking electrical feedthrough. The result will be cooling and thermal contraction of the vacuum vessels, so one needs allowance for that. Thus, not only for alignment and assembly, but also for thermal contraction, we will investigate the inclusion of vacuum bellows periodically in the vacuum vessel string.

The C^3 Demonstrator will run in two modes:

- Accelerator development where there will be minimal LN_2 flow. The LN_2 will be kept at nominal height above the accelerator sections, and nitrogen vapor will be vented.

- Vapor and liquid flow testing: LN_2 flow and vapor return between 2.5 and 10 kg/s. The actual flow rate will be determined by the power into the LN_2 boiler at the end of the cryomodule string opposite to the input cross, and the input LN_2 flow will be adjusted to maintain the LN_2 height in the cryomodules.

[1]The actual main linacs may contain partial super-sectors.

2023 JINST 18 P09040

The conceptual design is shown in figure 15 and consists of an electron source and injector that operates at 100 MeV followed by three cryomodules. The entry point for the cryogenic liquid is between the injector and the three cryomodules. After the three cryomodules a liquid nitrogen boiler is used to simulate the thermal load of a full super-sector with resistive heating. The boiler will consume power only during vapor and liquid flow testing.

LN_2 enters and vapor exits through a cross that will be a full prototype of a super-sector cross, see figure 18. LN_2 enters the bottom of the cross through a metering valve from a $\sim$ 50,000 liter LN_2 storage dewar kept at $\sim$ 80 K. The valve is controlled by the liquid level in the cryomodules, and feed forward control based on power dissipated in the liquid can be tested. Vapor exits from the top of the cross through a metering valve that is controlled to maintain $\sim$ 1.1 bar in the cryomodules.

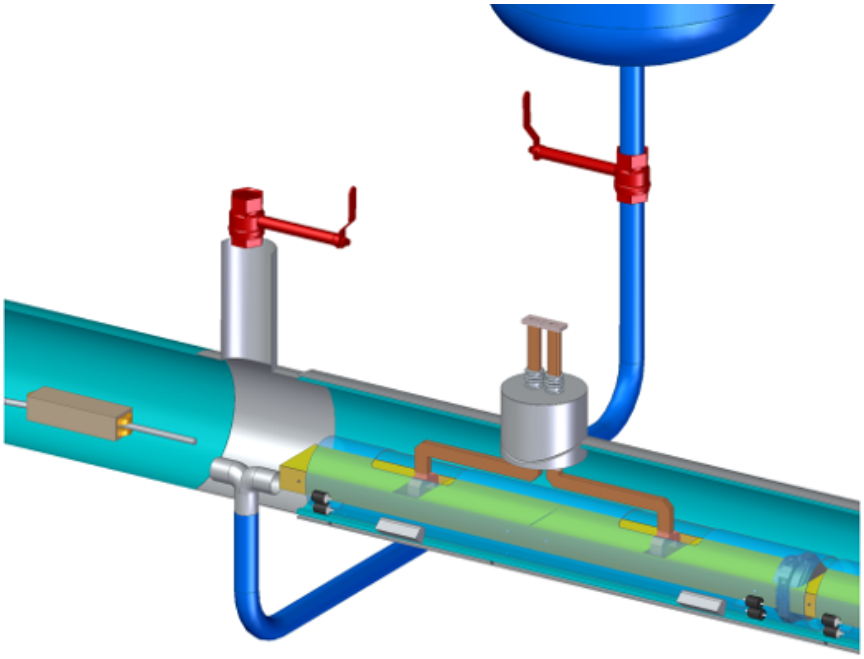

Figure 18. Rendering of the cross for inserting liquid nitrogen and removing nitrogen gas from the cryomodule. Liquid nitrogen comes in from bottom and is directed laterally in two counter propagating directions. The inlet control valve regulates on liquid level and is capable of supplying the full liquid flow rate envisioned for the C^3 main linac. The outlet valve regulates on the pressure of vapor in the cryomodules.

LN_2 fills the boiler at the downstream end of the cryomodules to the level in the cryomodules. During the first mode of operation, the heaters are off. For the second mode of operation, the heaters can be powered up to $\sim$ 2 MW, which will produce $\sim$ 10 kg/s of vapor. This will provide adequate margin for testing the system beyond expected flow rates.

We will pursue optical studies of nitrogen two-phase flow in the cryomodule to probe two-phase instabilities in the vessel. N_2 gas phase velocities corresponding to 10 kg/s mass flow can be high enough to initiate a surface wave instability on the LN_2 underneath the vapor. An optical setup such as a transparent window on the demonstrator vacuum and LN_2 vessels will help probe two-phase instabilities in the vessel. Alternately, cryogenic cameras can be housed inside the LN_2 vessel to capture images of LN_2 surface and determine gas velocities that lead to the instability. During a cold

2023 JINST 18 P09040

rf test, this optical setup will also provide information on nucleate boiling, for instance whether gas bubbles actually trap under the accelerator structure.

The S-band accelerator for the electron source of the demonstrator will also be in a cryomodule, and will be linked to the super-sector cross by a cryomodule containing the normal conducting bunch compressor. This will allow for the electron source linac topology to also be tested on the timeline of the C^3 Demonstration R&D Plan.

3.1.2 Cryomodule internals design

The Cryomodule functionality is:

- Provision of stable support for the accelerator sections and quadrupoles.
- Provision of the "cool" environment of $\sim 80\,\mathrm{K}$, including heat removal from the accelerators.
- Provision of alignment capability within a cryomodule, and to adjacent cryomodules.
- Provide feedthroughs for waveguides and other cables.
- Enabling of the above safely and reliably.

The basic mechanical building block is the "raft", see figure 19. A raft consists of two accelerator sections and a permanent magnet quadrupole. The quadrupole has an integrated cavity beam position monitor (BPM). The quadrupole design shown in figure 19 is based on a prototype developed by Electron Energy Corporation (EEC) with an innovative field adjustment mechanism using dynamically tunable magnets. EEC's design is engineered for immersion in LN_2 and enables a compact and uniquely flexible permanent magnet quadrupole that achieves the field requirements, superior to current designs, for C^3 . There are 4 rafts per cryomodule which is $\sim 9\,\mathrm{m}$ long. There are 10 cryomodules per sector, which is $\sim 100\,\mathrm{m}$ long. Finally there are 10 sectors per super-sector, which is $\sim 1\,\mathrm{km}$ long. The C^3 Demonstration R&D Plan calls for three cryomodules to be tested in series. The cryomodule will fit in a standard ISO shipping container (40 feet long).

The raft components are held by a channel which is a very open truss structure. The two accelerators and the quadrupole are pre-aligned on the raft. These components have 5 degrees of freedom (d.o.f.), with Z constrained by a ball in a groove at each midpoint. The raft is suspended from piezoelectric transducer stacks with a range of 200 microns and a bandwidth of $\sim 100\,\mathrm{Hz}$. These actuators are for beam based alignment and dynamic feedback. The transducers are an intermediate stage suspended from high resolution cryogenic electric motor jacks, with a range of $\sim 2\,\mathrm{mm}$. These jacks are primarily for inter-raft alignment, including the cryomodule transitions. It is expected that they would rarely be used after initial alignment unless there are upsets such as earthquakes. The motors are unusual in that they can be dirty in the sense of throwing off particulates, and only need a minimal bearing lifetime. A cross section of the cryomodule showing the accelerating structure, the waveguide feed, support raft, quadrupole, mechanical and piezoelectric movers, and stretched wire aligners is shown in figure 20.

The cryostat is a vacuum insulated pair of concentric cylinders, with a 30 cm inner radius of the cold cryostat. The cold cryostat will (probably) be made of 304 stainless steel, which closely matches the integrated thermal contraction of Cu. The outer cryostat can be soft steel. The inner

2023 JINST 18 P09040

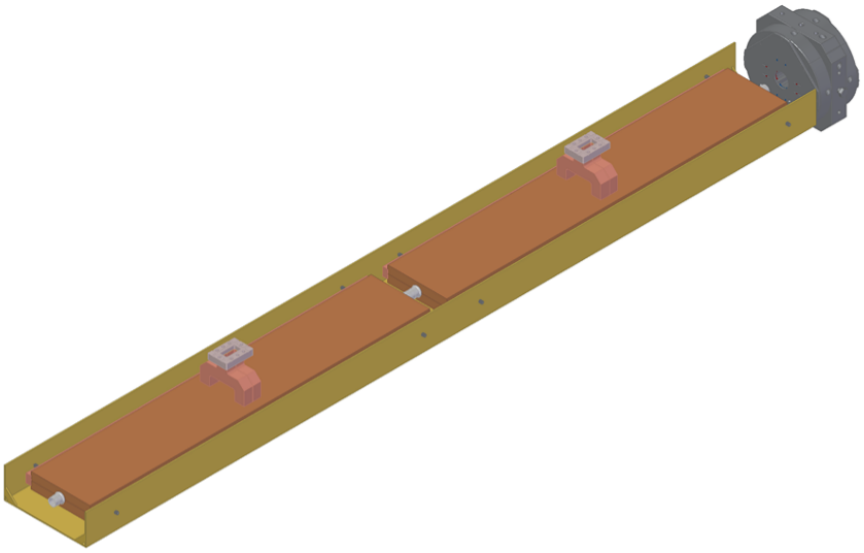

Figure 19. Rendering of the 2 m C^3 support raft with 2 one meter structures and one permanent magnetic quadrupole.

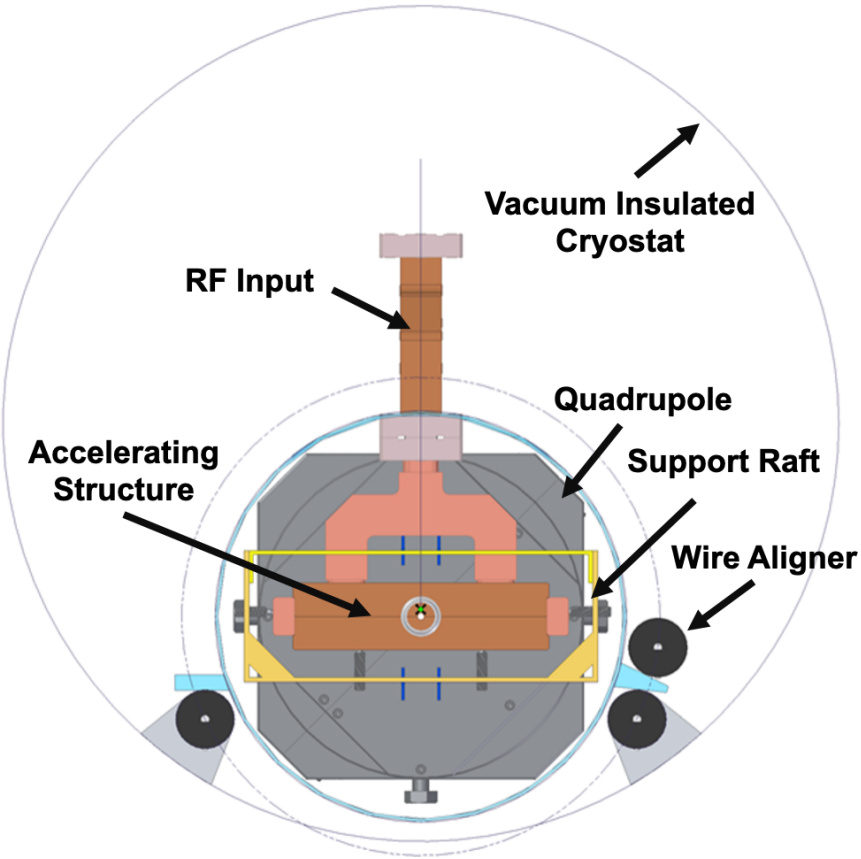

Figure 20. Rendering of the cryomodule cross section. In this view the accelerating structure, the waveguide feed, support raft, quadrupole, mechanical and piezoelectric movers, and stretched wire aligners are visible.

2023 JINST 18 P09040

cryostat will be wrapped with Multi-Layer-Insulation (MLI). Each accelerator section is fed by one waveguide, and the two waveguides from one raft are routed together through a port. That port also accommodates cables for the alignment motors, transducers, alignment sensors, the BPM signals, and the quadrupole controls.

A pre-conceptual plan for the assembly of the waveguide ports exists. It is hoped that all connections associated with cryomodule are welded, avoiding all bolted flanges. The weld preps would be designed for cutting ("can opener") or grinding in case access were needed.

The integrated thermal contraction from room temperature to ~ 80 K is −0.31% for Cu and −0.29% for SS304. Therefore the ΔL between 1 m of Cu accelerator and 1 m of SS304 raft is ~ 200 µm. Thus the accelerator midpoints are pinned to the stainless and the accelerator sections separate by 200 µm. This ΔL is taken by bellows on the beam pipes between accelrating structures.

The 9 m SS304 inner cryostat contracts ~ 3 cm. Since the outer steel shell stays warm, sliding support is needed. The adjacent cryomodule inner cryostats separate by 3 cm. This ΔL is taken by bellows between the two shells. The outer cryostats do not require bellows.

Table 3. Rf power losses in the accelerator structures for 4 considered C^3 scenarios.

Gradient (MV/m)	Power diss. (W)	rf flat top (ns)	Pulse compr.	Comments	Power/area (W/cm^2)	ΔT Cu-bulk to LN_2 (K)
70	2500	700	N	C^3-250	0.393	2.3
120	2500	250	N	C^3-550	0.393	2.3
155	3900	250	N	C^3-550 in 7 km	0.614	2.5
120	1650	250	Y	C^3-550	0.259	2.1

The rf thermal loads are shown in table 3. For C^3-250 and C^3-550, the loads are 2500 W per accelerator section. If C^3-550 is forced into 7 km, then the load will go up to 3900 W per section. If rf pulse compression is added, the thermal load can be reduced to 1650 W per section. A goal of the Demonstrator is to show that this range of loads can be handled without causing vibration problems at the flow rates required for full super-sector flows, i.e. going up to 10 kg/s of Nitrogen. These power dissipation values correspond to loads between 0.26 and 0.61 W/cm^2, which are in the nucleate boiling regime. The expected ΔT is below 2.5 K.

3.1.3 Cryomodule assembly

It seems likely that the cryostat consisting of cold and warm tubes plus the wave guide ports and inter-module connections can be commercially procured for the Demonstrator. The cryostat would also be fitted with the sliding supports for contraction of the cold tube. This cryostat would be leak tested warm and shipped to the assembly site in an ISO container fitted with suitable restraints.

Rafts will be assembled and aligned on a 5 m granite table placed so the rafts can be coupled together and pulled into the cryostat along with their alignment wires. It will be possible to adjust the alignment wires by reaching through the waveguide ports. All the remote alignment systems (motor driven jacks and piezo transducers) will be tested before raft insertion. Each raft will have a locking feature to the cold cryostat for transport that is accessible from the cryostat ends. These locks will be released before final placement of the cryomodules on the beamline.

2023 JINST 18 P09040

3.1.4 Beam dynamics

There are some key beam dynamics studies required to fully validate the new style of distributed coupled structures. Following a program similar to NLC in the past, the impact of short and long range wakefields on the accelerated electron and positron beams need to be studied in comprehensive start-to-end tracking simulations, with associated experimental tests at the demonstration facility to qualify the expected wakefield kick factors. Such an experimental demonstration would closely follow measurements made for the NLC program at the NLCTA test facility [51]. A magnetic spectrometer following the C^3 accelerating structures can be used to determine the beam energy and energy spread and bunch-to-bunch offsets. A kicker in the out-of-bend plane can provide the ability to separate the bunches to allow independent measurement along the bunch train. Optics before the chicane will be implemented, along with profile measurement devices, to infer the emittance of the beam.

Vibration and alignment tolerances are also a key consideration. Again, tolerance calculations will follow from start-to-end simulations, including the beam delivery system, which include such dynamic error sources and associated beam-based feedback systems. Experimental validation of the alignment of structures and magnets, together with direct measurement of structure vibrations and the direct impact on the measured beam properties at the demonstration facility will directly feed into these simulations. The demonstration facility beam measurement suite will also be utilized to directly measure the impact of observed breakdown events in the structures.

3.1.5 DC polarized electron gun and injector

The baseline electron (polarized) and positron (unpolarized) sources for C^3 are conventional linear collider designs. For the electron source, this consists of a polarized DC gun, buncher and accelerator. Extensive development has been undertaken for a DC polarized electron source that is able to meet the requirements for a linear collider (including the parameters required C^3) [52, 53]. The baseline plan for the C^3 demonstration does not incorporate the testing of a DC electron source with the cryomodules. However, as the design of the C^3 collider progresses, the DC guns that have been designed will need to be revisited for the specific parameters of C^3 . If it is deemed necessary to test the acceleration of the beam to a few GeV, the C^3 demonstration facility would be a suitable facility for doing so. In addition to a DC gun as the electron source for C^3 , we are also exploring the possibility of a polarized rf photo-injector and it would be the target for this demonstration plan to incorporate such a (unpolarized) photo-injector first.

3.1.6 High-brightness polarized emitters

All proposed future e^+e^- colliders including C^3 require an electron source with a high degree of spin polarization. The current state-of-the-art polarized electron source remains GaAs activated to negative electron affinity with a sub-monolayer of Cs and O_2 or NF_3. Several critical advancements have improved performance beyond that of bulk GaAs: superlattice structures have been shown to both dramatically enhance electron spin polarization [54], and the inclusion of a Fabry-Perot-style optical resonator via additional layered structures significantly enhances quantum efficiency by increasing absorption [55]. However, perhaps the most challenging aspect using GaAs photocathodes still remains: the Cs-containing activating layer is extremely sensitive to oxidation, preventing use in all but extreme high vacuum ($P < 1\times^{-10}$ Torr).

2023 JINST 18 P09040

Research in photocathodes devotes significant effort to the growth and characterization of high quantum efficiency semiconductor materials, including ongoing work at the Center for Bright Beams (CBB), a multi-institutional National Science Foundation Science and Technology Center focused on high brightness electron beam science. Among these, both Cs_3Sb and Cs2Te have been shown to be able to activate GaAs to negative electron affinity. When grown thin enough, this activating layer preserves the high electron spin polarization of superlattice GaAs [56]. Critically, while both Cs_3Sb and Cs_2Te must also be operated in pure vacuum, they are far more robust than the previous monolayer Cs-based coatings; in low-voltage test chambers, these spin-preserving activating layers have been shown to have significantly longer lifetimes [57].

The cryocooled copper technology that underpins C^3 enables the possibility of a very high field photocathode rf gun (photocathode field in excess of 240 MV/m), with a brightness that potentially eliminates the need for an electron damping ring. As the lifetime of polarized GaAs photocathodes is largely determined by the integrity of the activating layer, it will be critical to test these longer-lifetime activating materials in high extraction field for lifetime, dark current, and intrinsic emittance. CBB researchers are actively collaborating to test photocathodes grown at Cornell in the high field photocathode rf guns at UCLA. CBB also actively investigates other novel photocathode protection coatings, such as 2D materials, which may further improve lifetime in extreme accelerator environments.

CBB researchers also actively investigate the performance of cryogenic rf cavities. The primary cryogenic testing infrastructure for CBB is housed at Cornell University. Beyond CBB, the Cornell SRF group has decades of experience with in-house design, testing, and construction of superconducting RF cavities and full cryomodule cooled to 2 K. The Cornell SRF group has also pioneered several novel material approaches to cryogenic rf cavities, including demonstrating superconducting Nb_3Sb cavity coatings with very high quality factor which can operate at significantly higher temperatures than Nb-only SRF cavities. Dark current is a critical limiting factor for accelerating structures operating at the extreme gradient limit. Cornell is well-suited for the investigation of surface preparation techniques that mitigate dark current at cryogenic temperatures, as well as surface coatings that passivate field emission or increase the quality factor of the structure, thereby limiting the energy dissipated in the cavity thus potentially the breakdown rate. There are also CBB-sponsored activities at UCLA, embracing mainly ultra-high field and cryogenic cavity issues.

3.2 High power klystron upgrades

The high power rf system for the initial demonstrator will consist of commercially available 50 MW C-band klystrons and modulators; 18 klystrons are required. To provide a path for full scale implementation, it is necessary to adopt the latest innovations for rf source design leading to increased rf source efficiency and power at equivalent or reduced construction costs. Indeed, for a full-scale collider, the fabrication and installation costs of the high power rf system can be comparable to that of the tunnel and accelerating structure itself. In the near term, efficiency improvements can be had by designing an optimized rf circuit. Techniques for maximizing klystron efficiency, such as the Core Oscillation Method (COM), were explored in depth through the High Efficiency International Klystron Activity (HEIKA), yielding klystron efficiencies up to 80% at X-band; these same methods could be deployed at C-band. [95] Fabrication and operation costs may be reduced further by replacing the conventional solenoid focusing with a periodic permanent magnet (PPM) focusing structure that

2023 JINST 18 P09040

leverages existing mass-produced magnets. Efficiency can be increased further by incorporating PPM focusing within a multi-beam device to reduce the effective perveance of the device. Finally, advances in commercially available additive manufacturing will be evaluated for rf sources, and may be incorporated in low-risk assemblies (for example, in "dressing" assemblies outside the vacuum envelope) when such an approach can lead to substantial fabrication cost reductions.

3.2.1 Low level rf and klystron controls

The rf phase requirements of 0.1% and 0.3° C-band phase (150 femtoseconds) are comparable to the requirements of 4th generation light sources. A recently developed Low Level rf (LLRF) system at SLAC provided < 20 femtosecond RMS drive noise and < 5 femtosecond RMS readback noise in a 1 MHz bandwidth, considerably better than required for C^3 . The klystron modulator interlocks are comparable to those on existing accelerators.

Neither the LLRF or rf controls require any new technology in order to meet the C^3 requirements, and any development would be directed at reducing cost. As the underlying technology is rapidly evolving, detailed designs for both the C^3 demonstration and the collider should be delayed until there is a firm project schedule in order to allow use of the most recent technology. Its is likely that these systems will be based on highly integrated RF / FPGA / CPU parts such as the Xilinx RFSOC.

3.2.2 Precision timing/phase distribution

This is required in order to control the phase of the rf stations. Again the requirements are similar to those for 4th generation light sources and long distance phase stabilised rf over fiber systems are available commercially. The long distance fiber systems can be combined with local reflectometer based rf phase distribution similar to that used on LCLS-II. As with LLRF, this is a rapidly evolving technology and the design should be deferred until there is a firm project schedule. Systems to phase lock rf stations and mode locked lasers to rf phase references meeting these requirements have been used in accelerator/FEL systems at various laboratories.

3.2.3 Beam diagnostics

The beam diagnostics resolution requirements for C^3 are similar to those for 4th generation light sources, but with the additional requirement of closely spaced (few nanosecond) bunches.

Cavity BPMs are able to provide both high spatial resolution and with high bandwidth electronics can provide independent measurement of bunches in the train. Typically cavity BPM measurements are limited by mechanical stability rather than by the readout electronics. Note that the readout electronics could be identical to the LLRF electronics if high bandwidth RFSOC devices are used. Multi-bunch cavity BPMs operating under conditions where the bunch spacing is < cavity decay time, have been tested, but not used in production. The algorithm is straight forward: measure the change in vector field amplitude caused by each additional bunch in the train. There are tradeoffs between using cavities that are resonant with bunch rate which provide better train average position resolution, and using off-resonance cavities which provide better single bunch resolution.

Beam profile monitor technology will be driven by details of the accelerator design. Optical Transition Radiation monitors (OTR) provide high spatial resolution images, but cannot be used with beams with high longitudinal brightness due to coherent effects. In general they will function after a damping ring but not with a beam from an rf gun. The alternative of wire scanners can be

applied anywhere beam densities are not too large, but they provide only integrated, multi-bunch scans and are very slow. In areas where the charge density will destroy any type of intercepting diagnostic, laser wire scanners are the only known option.

Bunch arrival timing can be determined with rf pickup cavities that operate similarly to a BPM cavity. If a precision phase reference is provided, each BPM reference cavity can also serve as an arrival time monitor. This type of system has demonstrated < 10 femtosecond single pulse noise, easily sufficient for this application.

3.2.4 Accelerator raft alignment

The C^3 accelerating structures are supported by rafts. The rafts are responsible for providing a mechanism for alignment in warm and cold states with mechanical actuators and with piezoelectric feedback for beam based alignment. Each cryomodule contains 4 rafts; each raft supports two 1 m long accelerator sections and a quadrupole with mechanically integrated BPM. The accelerators and quads are attached to the raft with 5 d.o.f. ball joint adjustable tie rods, and are aligned on the bench before insertion into the cryostat. The Z position of the midpoint is mechanically fixed.

The rafts will have coarse and fine alignment, with each raft having 5 d.o.f. ball joint adjustable tie rods. The Z position of the midpoint is fixed. Each tie rod will have both a 200 micron travel piezoelectric actuator as shown in figure 21, and a magnetically coupled manual screw adjustment from outside the cryostat. The fine alignment of the rafts will be beam-based and dynamic with a bandwidth of ~ 100 Hz.

Figure 21. A 200 micron travel piezoelectric actuator. Actuators operate at cryogenic temperatures and high mechanical loading. The devices were developed for LCLS-II.

As a baseline, the coarse alignment of the rafts is done with stretched wires. Each wire is ~ 20 m long and spans two cryomodules, with the wires starting on successive cryomodules. Each raft has two wire position sensors for each wire, one on the first accelerator and the other on the quad. The sensors measure X and Y, with a precision of ≤ 100 microns. The rafts are slightly over-constrained with 8 measurements for 5 d.o.f.

The stretched wire method [58] is chosen since it must operate in air, vacuum, and under liquid nitrogen (rf off). Early-on in the demonstrator R&D plan stretched wire prototypes must be designed and tested for operation in liquid nitrogen, and to confirm that their performance is not degraded in this environment.

2023 JINST 18 P09040

Optical means of alignment provide significant potential advantages with operating over vastly different ranges with additional redundancy in the hardware. Rasnik is a 3-point alignment system [47]. This alignment is monitored by fixing a back-illuminated coded mask on the inner detector, a lens on the middle detector, and an image pixel sensor on the outer detector. An image of the mask is projected, by the lens, onto the image pixel sensor. The alignment of the three detectors can be obtained by analysing the image data, and track sagittas can be corrected for.

We are presently pursuing the testing of a Rasnik alignment system in a liquid nitrogen environment [48]. Multiple point 'leap frog' alignment can realised by equipping each point with a chainplate carrying closely spaced a mask, a lens and an image sensor, such that any set of three (identical) chainplates in a row form a Rasnik system. With n chainplates, the alignment of any plate with respect to the outer two plates, can be recorded.

For the alignment of the > 2000 accelerator structures of the C^3 project, the system should be able to operate in vacuum and in an environment of LN_2 . Given the index of refraction of LN_2 ($n = 1.20$), lenses can't be applied. This problem is solved by replacing the back-illuminated coded mask by a monochromatic light source emitting spherical waves, and the lens by a zone plate. This results in a well-known Fraunhofer diffraction pattern as image: the position of the pattern on the sensor defines the alignment of three points as before. Here, each chainplate will be equipped with a VCSEL laser and an image pixel sensor, and the zone plate is made by cutting out a hole, or better, an optimised transparent pattern.

3.2.5 Vibrations

As noted, three stages of alignment are foreseen: initial alignment of the accelerators and quadrupole on the raft; alignment of the rafts with respect to each other by stretched wires; and finally beam based alignment. It is also required that structure vibrations be kept to acceptable levels. Vibrations can be driven by seismic disturbances [59]. Prospective sites should be adequately quiet, and this has been studied by NLC, ILC, and CLIC. A new vibration source needs to be studied that arises from the nucleate boiling of liquid nitrogen and possibly the flow of nitrogen vapor. Preliminary measurements were started with a dummy accelerator fitted with 3 cryogenic accelerometers along the 3 axes, with everything under LN_2, and a small heater in the Cu slab. The test bed for experimenting with vibrations induced from thermal loads is shown in figure 22.

The continuation of this study should be done before substantially more design work is completed. Bubble formation and particularly bubble aggregation under the accelerator at high thermal loads should be studied to understand margins. This should utilize direct optical observation of the accelerator surfaces as well as accelerometer measurements.

3.2.6 High power rf distribution

- *Specification of waveguide network*

  This section describes the high power rf distribution system at C-band (5.712 GHz). The system transmits rf pulse power from the klystrons to accelerating structure. The rf distribution system will provide for monitoring the pulse power level of the klystron output. The major specifications of the waveguide network are shown in table 4.

2023 JINST 18 P09040

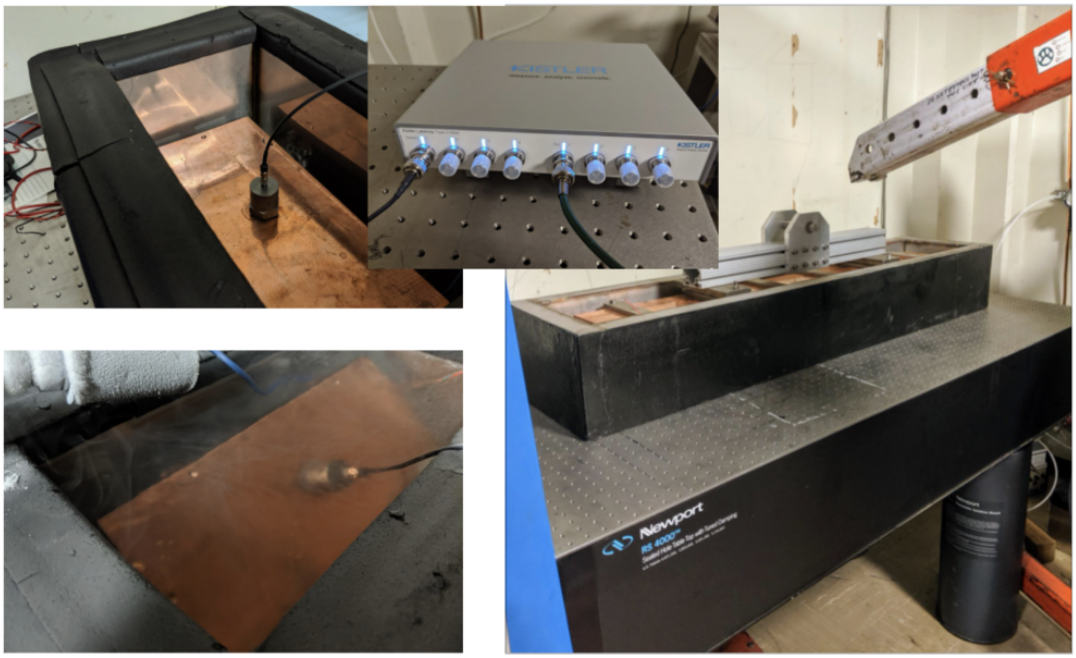

Figure 22. Test bed for measuring vibrations from the boiling of liquid nitrogen due to applied thermal load in copper structure.

Table 4. Specifications for the waveguide power distribution network.

Operating frequency (MHz) 5712
Waveguide Scattering Coefficient (S_{11}) less than 0.07
RF peak power (MW) 80
RF average power (kW) 20
Phase deviations of output RF power relative to an input reference phase (deg) less than 3
Vacuum operating level (Torr) 10×10^{-7} at full rf power and 10×10^{-8} at zero rf power
Gas burst rate (Rate) Less than 1 burst per hour average at full RF peak power after conditioning

An initial condition for the design of the waveguide network is based on the decision to feed each standing wave structure raft from one klystron. In this case, the first step of the rf phasing can be made at a low level rf drive signal and less accuracy is needed for the waveguide temperature stability. The precision adjustment of the accelerating rf phase is performed by a phase shifter installed in each waveguide branch. A simplified rf network layout is shown in figure 23. The rf network layout is indicated with flanges connecting hardware components. Evaluating which of these we can replace with welds will be one of the activities for the C^3 Demonstration R&D Plan.

The waveguide system will be designed to operate in high vacuum. This decision dictates developing of reliable vacuum directional couplers, power splitters, vacuum pumpout orifices with a high conductance and negligible rf coupling. The primary elements affecting the waveguide layout will also include the mechanical sub-system allowing rapid replacement

2023 JINST 18 P09040

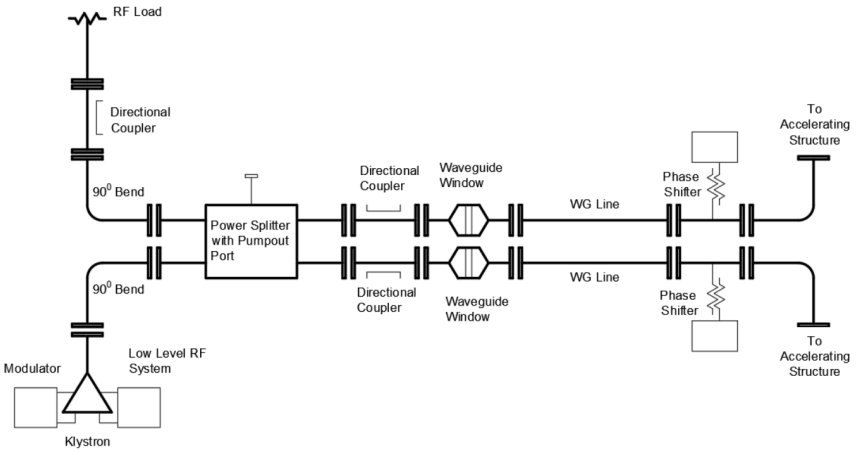

Figure 23. Schematic of the high-power rf waveguide distribution network. The configuration shown is for one klystron feeding a 2 m raft.

of the klystron. The overall C^3 rf distribution design philosophy is targeted at allowing the replacement of the klystron without significant work at the waveguide network.

Three standard waveguides can be used to transmit RF power from the klystron to the accelerating section. They are WR137, WR159, and WR187.

Specification of their inside dimensions is as follows:

- WR137 inside dimensions: $1.372'' \times 0.622''$
- WR159 inside dimensions: $1.59'' \times 0.795''$
- WR187 inside dimensions: $1.872'' \times 0.872''$

Maximum rf power transmitted via oxygen-free high conductivity (OFHC) copper WR187 waveguide may be up to 350 MW peak in vacuum [60]. High-power experiments have shown that the main reason for the rf breakdown is a poor-quality inner waveguide surface. The waveguide thickness of $0.157''$ is enough for easy machining and assembling for the brazing process. The $0.157''$ waveguide thickness may be chosen to allow using a common jig to join each element in the brazing process. Typically, a dimensional accuracy of less ±40 mils is acceptable.

The theoretical attenuation constant in WR187 is 3.635 mNp/m. It corresponds to the 0.032 dB/m transmission losses at room temperature. A preliminary length of each waveguide branch from the klystron to the cryomodule input is 30 ft (approximately 10 m). An average RF power loss in the copper WR187 waveguide will be less than 1.5 kW in this case.

- *RF Flange*

An important issue to address is the design and adoption of a standardized waveguide vacuum flange. This important component must serve in two roles as both an rf seal and a vacuum seal. The VSWR of the joint must be less than 1.015 at a frequency 5712 ± 50 MHz. The flange pair should be capable of transmitting 160 MW peak RF power. A leak rate should be

2023 JINST 18 P09040

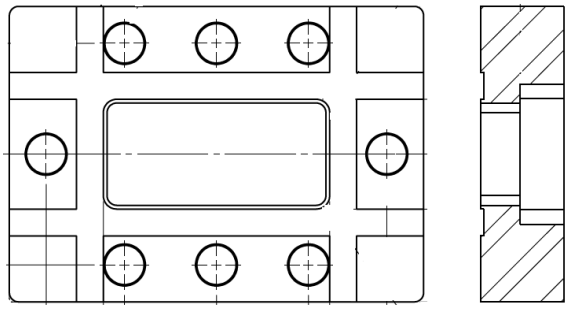

Figure 24. Schematic of the face and profile of a RIKEN-DESY WR187 flange.

less than $^{2} \times 10{-}10$ std cm^{3} He/s. The completed seal should be leak tight when the assembly is subject to a bake-out cycle consisting of heating at rate of 100°C/hr to a peak of 560°C, holding at this temperature for 48 hours and cooling at a rate of 100°C/hr.

Further, the most commonly occurring problems such as discharge breakdown and vacuum leak often happen near the flange gasket.

A new type unisex waveguide flange has been developed at KEK [60] to increase reliability and reduce cost; it comes from the RIKEN-DESY WR187 flange as shown in figure 24.

- *RF Window*

  The average high-power klystron lifetimes are typically ~ 50k hours. The klystrons must be replaced in a case of its failure. The replacement work will be performed when a part of the vacuumed rf feeder is opened for disassembly of the klystron. The rest of the rf feeder will be under the vacuum. The rf window with the ceramic barrier is needed as an interface between an atmosphere and the vacuum envelope.

  The rf windows must reliably operate under 80 MW peak power levels. However, in the case full reflection from the accelerating section, the rf window must be working even with double rf power levels of the normal operating mode. A MW peak rf power produces an electrical stress inside the vacuum envelope and ceramic interface. RF breakdowns in these megawatt power environments could damage the rf window if the design is not done correctly. There are several innovations in the present rf window designs for S- and X- Band frequency ranges. Many of these innovations are practically realised. For example, the X-Band travelling wave mixed-mode rf window [61, 62] tested in the pulse mode up to 100 MW. The rf window for C-Band will be designed, tested, and optimized under ideas and innovations discussed in [63].

- *Power divider*

  One power divider will integrate into the waveguide network to split equally the output klystron power for two branches. A short-slot, narrow wall, coupled junction rf power divider is a tradition rf device that has been used in the high power rf systems. It has high power handling capacity and each of its ports lies in the same plane. The high power tests indicates that a short-slot divider can operate without rf breakdown at more than 70% of the power capacity of the terminal waveguides.

2023 JINST 18 P09040

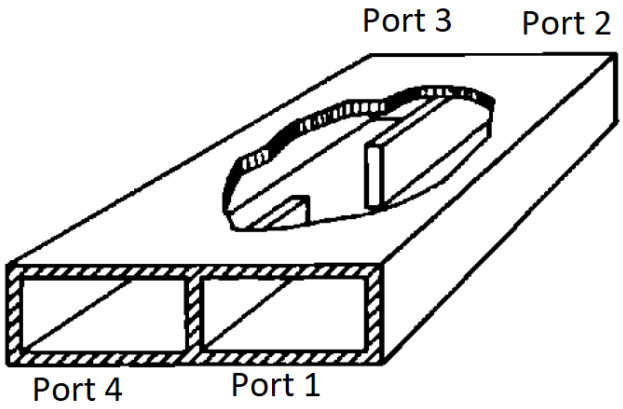

Figure 25. Schematic of a short-slot divider using two rectangular waveguides that share a narrow wall.

The basic construction of the short-slot divider uses two rectangular WR187 waveguides that share a narrow wall. Between them a single slot couples half of the incident power from one waveguide into the second guide. The two resulting waves are 90 degrees out of rf phase. A simplified sketch is shown in figure 25. The electrical phase length matching of both waveguide arms will be performed on the regular straight sections.

The C^3 accelerating structures operate in a standing wave. There will be a reflection of power from the structure back to the klystron. Part of the reflection power (ideally all) will propagate into Port 4. The high power vacuum dry rf load will absorb this power.

- *RF load*

  There are several concepts for high power load designs. Concepts may be classified by the class of rf absorption material to be employed. The most popular rf absorber that is used in the high power loads is water or other liquid lossy dielectrics. This load concept requires a solid dielectric interface separating the accelerating vacuum envelope and the liquid absorber. Such a concept is not acceptable for the C^3 demo because a catastrophic failure of one interface could destroy the long linac vacuum system; recovery from this failure would be expensive. As a result, the high power load concepts based on the liquid rf absorbers are not being considered. Our analysis will be focused on high power load concepts that are based on a multipactor-free concept with an advanced rf absorption materials capable of working in an UHV environment.

- *RF monitors*

  Modified Bethe hole direction couplers are a typical components that have been integrated into the waveguide network for rf power monitoring. The high power level in the waveguide requires the use of more than 60 dB coupling ratios. Three directional couples are shown in the rf feeder in figure 23. This figure represents a typical layout of one klystron station. Many couplers will be needed for the whole installation. A modified Bethe hole directional coupler is optimised to reduce their cost. The designs used allow for the insertion of a waveguide pump-out and vacuum gauge in the same space where a coaxial strip-line loop is placed. There are two types of designs of the couplers in the SLAC linac. These designs will be evaluated in

the C^3 demo. An employment of a dielectric window on the wide wave guide wall is used in the first coupler. This dielectric window is placed above the coupling hole and separates a vacuum atmosphere regions. The strip line loop is placed from the atmosphere side of the dielectric. Two vacuum rf feedthroughs are employed in the second concept. Both concepts are a subject for evaluation in the C^3 demo installation.

- *Phase shifter*

  One klystron feeds two accelerating sections in the present rf feeder layout. If the two waveguide branches of waveguide network are tuned properly, the rf power from the klystron into the input port of the power divider will arrive in phase at each of the two output ports. There is a transition located at the cryomodule for the waveguide to go into the LN_2 cryostat where the temperature will drop from room temperature to $\sim$ 80 K. The temperature decoupling in the waveguide is needed to reduce the thermal losses in the cryogenic vessel. There are several approaches for realizing this thermal break. One of them is to employ the thin-wall waveguide fabricated from a material with low thermal conductivity and low rf losses on the inner waveguide surfaces (for example with a thin copper coating). Inclusion of a phase shifter based on waveguide wall deformations will be evaluated in this space.

3.2.7 Start-to-end simulation

High fidelity start-to-end beam dynamics simulations were used in x-ray free electron laser light source accelerator design to verify and optimize the accelerator design concept [64–67]. This type of simulation should be carried out for the C^3 accelerator design too. Important physical effects such as three-dimensional space-charge, longitudinal and transverse wakefields, coherent and incoherent synchrotron radiation, and intrabeam scattering should be included in the simulation model. The effects of long-range wakefields on beam quality should also be studied. Machine imperfections such as misalignment errors and field amplitude and phase errors should be studied using the start-to-end simulation.

To provide the required luminosity for a linear collider, it is critical to reduce emittance dilution in the main linac from machine tolerances such as cavity misalignments and imperfections [68, 69]. For the C^3 linac, misalignments can arise from individual cavity misalignments and changes in the properties of coupled HOMs in a cryomodule with misaligned and deformed C^3 cavities. The rf parameters and fields of the HOMs can be evaluated for random distributions of cavity offsets (in a cryomodule) and cavity deformations along the full linac. The fields are then used for beam emittance dilution evaluation. A statistical analysis using the constraints form realistic fabrication and component placement tolerances will be facilitated by the HPC capabilities of advanced simulation codes [70].

Dark current and capture may have deleterious effects on the particle detector in the form of unwanted backgrounds. Integrated simulations using rf and beam dynamics codes will provide the needed tool for start-to-end simulation for linear colliders. The simulation starts with electrons emitted from cavity walls governed by field emission and their subsequent movements are tracked under the influence of the cavity accelerating mode operating at a specified phase. Secondary emissions will be generated if some of the electrons hit the cavity wall. The exit electrons from the cavity will be used for beam tracking along the linac with magnet components from the lattice until

2023 JINST 18 P09040

they reach the next cavity. A pipeline workflow involving rf and beam dynamics simulations will be developed to facilitate start-to-end simulations.

4 Parallel research and development

4.1 Damping rings

One important issue in advanceing the damping ring R&D is the injection/extraction system for the train of bunches which are separated a few tens of nanoseconds. Powerful and fast solid-state switches driving a transmission line kicker are needed. They must work in a pulse mode and be capable of generating power from MW to GW and rise/fall time from 10× ps to 100 ns. There are practical physical effects that can overcome the speed limitation for commercially available off self-solid-state switches. For example:

- nonlinear ferromagnetic media
- solid-state electron-hole plasma in semiconductors

In both approaches the nonlinear characteristics of the switching media (ferromagnetic and semiconductor) are employed in the final stages of the pulser to form multi- MW level nanosecond pulses. The pulse dynamic processes in ferromagnetic and semiconducting materials can support a 1 MW/ns switching speed stably, reliable, and efficiently. This fact is confirmed by our pilot experiments. For example, the effect of the high-power switching speed in semiconductors diodes is shown in figure 26.

In this case diodes were fabricated with special doping gradients in Si-based wafers via a deep diffusion process.

The waveform shown in figure 26 demonstrates a 1.3 MW/ns switching speed continually running at 25 kHz repetition rate with less than 20 ps RMS time jitter. A development of physics basis of semiconductor behaviour for a generation of GW levels of nano- and sub-nano power swings would be useful for the development of the damping ring injection/extraction system in the C^3 machine.

We will explore a variety of ultra-wide band-gap (UWBG) semiconductors (diamond, SiC, etc.) which are of great interest for their efficiency, speed, thermal management and radiation resistance.

4.2 Beam delivery system and final focus (BDS/FF)

Mature designs exist for beam delivery systems with an electron or positron beam energy in the range of 125 GeV–1.5 TeV as part of the ILC and CLIC programs. C^3 will continue to leverage the significant effort in simulations and hardware tests that have been developed and carried out over the past 30 years in preparation for a future linear collider. Trade-offs exist in design length and aggressiveness of beam parameters (e.g. β^*, L^*). These manifest as tighter, more complex diagnostics/correction hardware (higher-order magnets, $<$ µm accuracy movers, BPMs etc) and more complex, slower online beam size tuning systems, limiting achievable luminosity. The design for the BDS and FF is complicated and time consuming to evaluate. To date, a final focus system with ILC levels of demagnification has been experimentally demonstrated [71], but not beyond. We will use caution when designing the BDS and FF for C^3 with the main goal of simplifying

2023 JINST 18 P09040

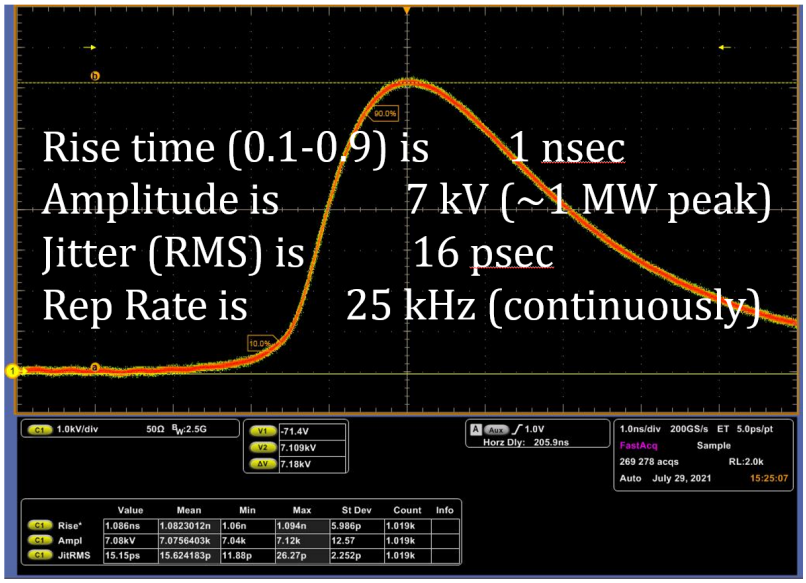

Figure 26. Demonstration of a 1 MW/ns switching speed.

and reducing the length of the BDS and FF. Pushing the design beyond key ILC FF parameters (principally, energy spread and final focusing doublet chromaticity $\sim L^*/\beta^*$) would require further experimental verification of performance.

The backbone for assessing the realistic luminosity potential of any linear collider is that of the start-to-end simulation (S2E). This should include a full description of the beam transport from the exit of the source (damping ring or rf photo-injector) through to the BDS and FF and to the collisions at the interaction point (IP). All relevant physics processes should be included: e.g., chromatic effects of magnets, short and long-range longitudinal and transverse wakefield kicks in accelerating structures, synchrotron radiation in bends, magnetic field errors and placement errors of all accelerator components. Both "static" misalignments and other errors as well as dynamic effects (errors which are fast on the timescale of corrective actions being applied) need to be considered. The BDS is especially sensitive to errors, containing diagnostics systems required by the physics detectors experimental program, and strongly non-linear beam dynamics with large multi-km beta functions, for example. Careful simulation with accurate descriptions of the various errors internally and input conditions from the linac are critical to assess the final performance of the collider. Extensive S2E simulation programs have been implemented in the past for the ILC and CLIC communities, with a strong focus on the FF tuning system [72]. It is envisioned to re-create such a community of beam dynamics simulation experts to generate a S2E simulation environment to assess the C^3 performance and form the basis for tolerance specifications.

The use of Machine Learning (ML) and Artifical Intelligence algorithms (AI) in the design and operation of particle accelerators is somewhat new and has not yet been fully explored for the field of next-generation linear colliders. The C^3 program should benefit from this rapidly advancing area of research. The BDS and FF are strongly non-linear systems which require complex tuning procedures to achieve full luminosity [72]: application of modern, multi-objective physics-informed Bayesian optimizers could yield powerful improvements in tuning performance and speed, possibly

2023 JINST 18 P09040

increasing confidence in an ability to push on the FF parameters. This would manifest in either an increased luminosity performance or operation at a similar luminosity with reduced beam power requirement (cost). Another example application of ML/AI technology could be applied to the problem of reconstructing beam aberrations at the IP collision using a combination of "event shapes" reconstructed using "beamstrahlung" monitors situated close to the IP [73]. Again, such technology could help with the accuracy of the beam tuning process yielding increased tuning speed, whilst also providing useful information to the detector community.

As exhaustive experimental tests have shown, at ATF2 [71], and FFTB [74] before it, despite the highly non-linear design aspects and complex tuning procedures, modern optics design and beam dynamics software is well capable of accurately describing the BDS and FF systems. Whilst there is always value added in test facilities, a test final focus system demonstration for C^3 is likely unnecessary as it does not strongly deviate from existing designs for the BDS/FF. A possible exception is the particular case of the FF design for the γ-γ design (XCC) [50]. This option requires the focusing of a round-beam configuration, necessitating a final triplet configuration of magnets which has not yet been designed or studied for small-beta focusing optics required at a linear collider. One possibility to demonstrate this configuration for the FF might be a future upgrade to the FACET-II [75] Sector 20 experimental region which already operates with round-beams ($E = 10\,\text{GeV}$, $\beta^* > 5\,\text{cm}$, $s_z < 1\,\mu\text{m}$, $Q < 2\,\text{nC}$). Further novel aspects of the XCC concept which demand a fresh look at the BDS design include the integration of keV energy x-ray focusing optics to overlap with the electron beams close to the IP and generate the colliding gamma beams. Consideration of FF optics which pushes substantially beyond that already demonstrated can be beneficial in terms of cost savings and/or luminosity performance. The premier facility in the world for such experimental studies is ATF2 at KEK: whilst the accelerator is currently still operating, serious further investment would be required to enable a program to experimentally verify such pushed parameters are feasible.

4.3 Levitated positron target — radiatively cooled

Positron sources are based on electron or photon beam striking a high-Z target, often W. Because both the instantaneous and average power are high, the concept of a rotating Ti hoop in the accelerator vacuum is being considered [76]. The the ILC baseline, water cooling introduced through rotating seals, and rotating seals are used for an axial drive shaft. A concept has been proposed [77] using radiation cooling of high performance Ti alloy blades to a water cooled vacuum can, completely eliminating water channels in the vacuum space has been proposed. In addition, a concept for magnetic suspension and drive of the hoop, eliminating shaft seals, that does not require permanent magnets, and so should survive in the high radiation field of the target is also being explored. Increasing the reliability and performance of the positron target would have significant benefits for C^3 operation and advancing this concept will be explored.

4.4 Advanced rf source research and development

With the development of this highly efficient linac topology, we expanded our vision for a future high gradient linac architecture that comprises a much more simplified RF system with a great deal of optimization for the cost of the peak power generation. A central tenant of the C^3 concept is a rf only upgrade to increase the energy from 250 GeV to 550 GeV CoM. This upgrade affords us the opportunity to implement novel concepts for the rf sources that will be used for the upgrade. To this

2023 JINST 18 P09040

end, we are proposing a very simple, modular system with an order of magnitude cost reduction for the accelerator complex. The idea starts with developing low voltage RF sources with extremely high efficiency, which translates to a low current and lower power. To get to high power, we utilize the narrow bandwidth of the system, which allows us to design an efficient combining network for a large number of low voltage systems. This, in turn, leads to inexpensive, relatively low voltage modulators and hence fast rise and fall times, eliminating the need for pulse compression. With a large number of small tubes, mass production cost reduction could result in substantial savings.

To realize this vision, we need to have a comprehensive program for these advanced microwave rf sources [78–81] with the end goal of an experimental demonstration of C-band modular multi-beam klystrons with efficiencies $\geq$ 65%, with periodic permanent magnet (PPM) focusing and high power. This should be followed by a demonstration of the combining mechanism; many methodologies are possible, but there is a new invention for combining with a two-dimensional Floquet network; a 16 tube combiner has already been demonstrated [23]. Finally, a demonstration of a fully integrated tube with suitable power combination operating with efficiency $\geq$65% should follow.

4.5 RF pulse compression

Another possible upgrade to the C^3 concept is the implementation of rf pulse compression. RF pulse compression can decrease the fill time and thermal load into the cryogenic vessel. Given the efficiency of cooling at cryogenic temperatures of $\sim$ 80 K (approximately 15%) this can have a significant impact on the cost and operational efficiency for the complex. A compression of 3$\times$ for the filling portion of the rf pulse has been shown to have tremendous benefits [41]. The development of pulse compressors for cryogenic linacs that meet this level of compression is an ongoing topic of R&D, as noted in the discussion of Very High Energy Electron therapy systems in a concurrent submission to Snowmass 2021 on FLASH Radiation Therapy [82, 83]. RF pulse compression has been used extensively for large scale accelerator applications to supply short high peak power pulses with cost efficient long pulse, low power sources [84]. Recent innovations in RF compressor cavity design have enabled a dramatic reduction in the system footprint while maintaining the capability to produce 6-fold pulse compression and isolate the source from the reflected RF signal from the cavities. [85, 86] For cryogenic copper structures, cavity designs will need to achieve high intrinsic quality factors, Q_0 up to 400,000, and high coupling factors, β up to 10. Active research in this area will continue to benefit the broader accelerator community that relies on pulse compressors to supply the peak powers needed for high gradient operation. Indeed, the development of accelerator technology needed for C^3, from the distributed-coupling linac design at cryogenic temperatures to potential pulse compression for high-efficiency operation, will have a cross-cutting impact in support of efforts to design compact, cost-efficient accelerators for medical and security applications.

4.6 Industrialization

As with any linear collider designs the volume of hardware production that will be required is a daunting task for C^3. In an effort to render the required production practical we will strive to engage with the existing and emerging accelerator technology sector and related technological sectors that will be required for C^3. Fortunately, the production of hardware directly applicable to a normal conducting rf accelerator is already quite significant. This is in large part driven by the demand for medical and industrial accelerators that produce high-flux x-rays. For example, in less than a decade

2023 JINST 18 P09040

from the launch of Varian's flagship radiation therapy model, one company built and installed the equivalent of a C^3 main linac in hospitals all over the world. [87] If C^3 technology is successfully transitioned to the industrial sector not only will C^3 benefit from industrial production, but commercial vendors will be able to offer more compact and higher efficiency accelerator and rf sources.

This potential exists beyond the direct accelerator technology sector. For example, one of the key advantages of the C^3 accelerating structure is the minimization of part count, a robustness of manufacturing through CNC end milling of split block structures, and use of bonding techniques that minimize the possible impacts on structure performance. While commercial vendors are presently integrated in the production of linac components, increasing the rate of fabrication, reducing part-to-part variability, automating tuning and diversifying the supply chain are all topics to be explored during the demonstrator R&D plan. The production of accelerating structures for three cryomodules, individual structure tests and the injector, will allow for a broader engagement with manufacturing industry (in particular small-business machine shops with aerospace experience).

The RF sources (klystrons) are expected to be significant cost drivers for any future accelerator facility, and C^3 is no different in this regard. To drive down klystron procurement costs, commercial partners should be engaged as soon as possible in the development effort. There should be robust support for a public-private collaboration to evaluate the most cost-effective path forward. A few options could be considered, depending on the available infrastructure, tradeoff between lab-run or supplier-run operations, and the capabilities of industrial partners:

- Klystron design, fabrication, and test entirely by multiple commercial partners. It is important to ensure simple interchangeability of sources in this situation.
- Klystron design completed by government labs; klystrons built-to-print, tested, installed, and maintained by commercial partners.
- Klystron design completed by government labs; built-to-print by commercial partners; but tested, installed, and maintained by the C^3 facility.

Industrial R&D is driven by immediate and long-term market potential. From this viewpoint, a proposed future collider presents a significant risk that may not merit substantial investment in cost reduction and process improvements by industry. Therefore, in any partnership scenario, the industrialization effort should require — and financially support — a collaboration with government labs to evaluate and improve upon manufacturing processes. When the most economical approach is to use existing fabrication methods, those methods should be leveraged. When process improvements can be made (for example, using additive manufacturing to reduce part counts, or automation of testing processes), the investment required for industry to implement these changes should be supported directly. This provides a "win-win" scenario where the klystron costs for the future C^3 klystrons are reduced, and commercial partners can benefit from cost reduction measures which are broadly applicable and attractive to industry participants regardless of the timetable for the C^3 machine itself.

With this in mind, during the C^3 Demonstration R&D timeline (and in many cases presently ongoing) we will directly engage with industry in many technological areas: accelerator fabrication, beamline components, permanent magnets, vacuum vessel production, rf sources (klystron and modulator), LLRF, tunnelling, large scale cryogenics, etc.

2023 JINST 18 P09040

5 Conclusions

We present an update and proposed plans for R&D towards a cold copper (cryogenic) distributed coupling linear e^+e^- collider that can provide a rapid route to precision Higgs physics with a compact 8 km footprint. C^3 is based on recent advances in copper accelerator technology that allow robust designs with an accelerating gradient of 120 MeV/m. C^3 follows a program very similar to that proposed for the ILC, aiming at collecting data at 250 and 550 GeV in the center of mass, with a relatively inexpensive upgrade on the same footprint. We thus expect to achieve precision measurements of similar quality to those discussed for ILC and other e^+e^- Higgs factories. This program, starting before 2040, and possibly coincident with the end of the HL-LHC run, will achieve the goals of precision Higgs boson and top quark measurement at which one could realistically prove the presence of deviations from the SM. At the same time, C^3 will also provide the first step toward the extension of e^+e^- physics into the multi-TeV energy range.

The primary goal of the C^3 Demonstration R&D Plan is to reduce technical and cost risk by building and operating the key components of C^3 at an adequate scale. This R&D plan starts with the engineering design, and demonstration of one cryomodule and will culminate in the construction of a 3 cryomodule linac with pre-production prototypes. This work will be critical to confirm the suitability of the C^3 beam parameters for the physics reach and detector performance in preparation for a Conceptual Design Report (CDR), as well as for follow-on technology development and industrialization.

The successful full demonstration of the 3 cryomodules to deliver up to a 3 GeV beam and achieve the C^3-550 gradient will allow a comprehensive and robust evaluation of the technical design of C^3 as well as mitigate technical, schedule, and cost risks required to proceed with a Technical Design Report (TDR).

Acknowledgments

We are grateful to Fermilab Site Filler Collider working group, Sridhara Dasu, JoAnne Hewett, Tor O. Raubenheimer, Hirohisa A. Tanaka and SiD exectutive committee for their interest and encouragement. We would thank Nan Phinney for the careful revision of the manuscript. The work of the SLAC authors is supported by the US Department of Energy under contract DE-AC02-76SF00515.

References

[1] C. Vernieri et al., *A "Cool" route to the Higgs boson and beyond. The Cool Copper Collider*, 2023 *JINST* **18** P07053.

[2] S. Dasu et al., *Strategy for Understanding the Higgs Physics: The Cool Copper Collider*, in the proceedings of the *Snowmass 2021* [arXiv:2203.07646].

[3] M. Bai et al., *C^3: A "Cool" Route to the Higgs Boson and Beyond*, in the proceedings of the *Snowmass 2021* [arXiv:2110.15800].

[4] K.L. Bane et al., *An Advanced NCRF Linac Concept for a High Energy e^+e^- Linear Collider*, arXiv:1807.10195.

2023 JINST 18 P09040

[5] M. Nasr et al., *Experimental demonstration of particle acceleration with normal conducting accelerating structure at cryogenic temperature*, *Phys. Rev. Accel. Beams* **24** (2021) 093201 [arXiv:2011.00391].

[6] International Committee on Future Accelerators (ICFA), *ICFA Statement on the ILC Project*, 2020.

[7] European Strategy Group, *2020 Update of the European Strategy for Particle Physics (Brochure)*, http://cds.cern.ch/record/2721370 [DOI:10.17181/CERN.JSC6.W89E].

[8] J.N. Butler et al., *Report of the 2021 U.S. Community Study on the Future of Particle Physics (Snowmass 2021) Summary Chapter*, in the proceedings of the *Snowmass 2021* [arXiv:2301.06581].

[9] M. Narain et al., *The Future of US Particle Physics — The Snowmass 2021 Energy Frontier Report*, arXiv:2211.11084.

[10] S. Gourlay et al., *Snowmass'21 Accelerator Frontier Report*, arXiv:2209.14136.

[11] M.C. Llatas et al., *Report of the Snowmass 2021 e^+e^--Collider Forum*, arXiv:2209.03472.

[12] T. Roser et al., *On the feasibility of future colliders: report of the Snowmass'21 Implementation Task Force*, 2023 *JINST* **18** P05018 [arXiv:2208.06030].

[13] P. Bambade et al., *The International Linear Collider: A Global Project*, arXiv:1903.01629.

[14] FCC collaboration, *FCC-ee: The Lepton Collider: Future Circular Collider Conceptual Design Report Volume 2*, *Eur. Phys. J. ST* **228** (2019) 261.

[15] CEPC Study Group, *CEPC Conceptual Design Report: Volume 1 — Accelerator*, arXiv:1809.00285.

[16] CEPC Study Group, *CEPC Conceptual Design Report: Volume 2 — Physics & Detector*, arXiv:1811.10545.

[17] FCC collaboration, *FCC-hh: The Hadron Collider: Future Circular Collider Conceptual Design Report Volume 3*, *Eur. Phys. J. ST* **228** (2019) 755.

[18] D. Alesini et al., *Positron driven muon source for a muon collider*, arXiv:1905.05747.

[19] MICE collaboration, *Demonstration of cooling by the Muon Ionization Cooling Experiment*, *Nature* **578** (2020) 53 [arXiv:1907.08562].

[20] ALEGRO collaboration, *Towards an Advanced Linear International Collider*, arXiv:1901.10370.

[21] AWAKE collaboration, *Acceleration of electrons in the plasma wakefield of a proton bunch*, *Nature* **561** (2018) 363 [arXiv:1808.09759].

[22] *International Workshop on Breakdown Science and High Gradient Technology*, https://indico.fnal.gov/event/22025/.

[23] P.G. Maxim, S.G. Tantawi and B.W. Loo, *PHASER: A platform for clinical translation of FLASH cancer radiotherapy*, *Radiotherapy and Oncology* **139** (2019) 28.

[24] X. Lu et al., *A proton beam energy modulator for rapid proton therapy*, *Rev. Sci. Instrum.* **92** (2021) 024705.

[25] https://indico.cern.ch/event/939012/contributions/3971811/.

[26] https://indico.cern.ch/event/939012/contributions/3971198/.

[27] J.B. Rosenzweig et al., *An ultra-compact x-ray free-electron laser*, *New J. Phys.* **22** (2020) 093067 [arXiv:2003.06083].

2023 JINST 18 P09040

[28] F. Zimmermann et al., *Power Budgets and Performance Considerations for Future Higgs Factories*, *JACoW* **eeFACT2022** (2023) 256.

[29] W. Graves et al., *The ASU Compact XFEL Project*, *Bull. Am. Phys. Soc.* **65** (2020).

[30] M. Breidenbach et al., *A Sustainability Roadmap for C^3*, arXiv:2307.04084.

[31] W. Graves et al., *ASU Compact XFEL*, in the proceedings of the *38th International Free-Electron Laser Conference*, Santa Fe, NM, U.S.A., 20–25 August 2017, pp. 225–228 [DOI:10.18429/JACoW-FEL2017-TUB03].

[32] https://lhc-commissioning.web.cern.ch/schedule/LHC-long-term.htm.

[33] M. Cepeda et al., *Report from Working Group 2: Higgs Physics at the HL-LHC and HE-LHC*, *CERN Yellow Rep. Monogr.* **7** (2019) 221 [arXiv:1902.00134].

[34] J. de Blas et al., *Higgs Boson Studies at Future Particle Colliders*, *JHEP* **01** (2020) 139 [arXiv:1905.03764].

[35] J. Alison et al., *Higgs boson potential at colliders: Status and perspectives*, *Rev. Phys.* **5** (2020) 100045 [arXiv:1910.00012].

[36] K. Fujii et al., *Physics Case for the International Linear Collider*, arXiv:1506.05992.

[37] LCC Physics Working Group, *Tests of the Standard Model at the International Linear Collider*, arXiv:1908.11299.

[38] K. Fujii et al., *The role of positron polarization for the inital* 250 *GeV stage of the International Linear Collider*, arXiv:1801.02840.

[39] NLC Design Group, *Zeroth-order design report for the Next Linear Collider*, Tech. Rep. SLAC-R-474, SLAC, Stanford, CA (1996).

[40] CLIC accelerator collaboration, *The Compact Linear Collider (CLIC) — Project Implementation Plan*, arXiv:1903.08655 [DOI:10.23731/CYRM-2018-004].

[41] K.L. Bane et al., *An Advanced NCRF Linac Concept for a High Energy e^+e^- Linear Collider*, arXiv:1807.10195.

[42] Z. Li et al., *Optimization of the X-Band Structure for the JLC/NLC*, SLAC-PUB-11916, SLAC, Stanford, CA (2006).

[43] E. Nanni, *C 3 (Cool Copper Collider): An Advanced Concept for a Future Linear Collider*, *APS April Meeting Abstracts* **2022** (2022).

[44] https://indico.slac.stanford.edu/event/7467/contributions/5617/.

[45] https://indico.slac.stanford.edu/event/7467/contributions/5522/.

[46] https://indico.slac.stanford.edu/event/7467/contributions/6059/.

[47] H. van der Graaf et al., *The ultimate performance of the Rasnik 3-point alignment system*, *Nucl. Instrum. Meth. A* **1050** (2023) 168160 [arXiv:2104.03601].

[48] H. van der Graaf et al., *The alignment of the C3 Accelerator Structures with the Rasnik alignment system*, in the proceedings of the *International Workshop on Future Linear Colliders*, Menlo Park, CA, U.S.A., 15–19 May 2023 [arXiv:2307.07981].

[49] E. Prat et al., *Measurements of copper and cesium telluride cathodes in a radio-frequency photoinjector*, *Phys. Rev. ST Accel. Beams* **18** (2015) 043401.

2023 JINST 18 P09040

[50] T. Barklow et al., *XCC: An X-ray FEL-based $\gamma\gamma$ Collider Higgs Factory*, in the proceedings of the *Snowmass 2021* [arXiv:2203.08484].

[51] R.D. Ruth, *Contribution to IX international symposium on very high energy cosmic ray interactions (18-24Aug. 1996, Karlsruhe). Status and results from the next linear collider test accelerator*, SLAC-PUB-7386 SLAC, Stanford, CA (1996) [DOI:10.5170/CERN-1996-007.641].

[52] https://doi.org/10.22323/1.324.0014 J. Grames et al., *Milliampere Beam Studies using High Polarization Photocathodes at the CEBAF Photoinjector*, in the proceedings of the *XVII International Workshop on Polarized Sources*, Kaist, South Korea, 16–20 October 2017 [DOI:10.22323/1.324.0014].

[53] L. Rinolfi, *The CLIC Electron and Positron Polarized Sources*, in the proceedings of the *13th International Workshop on Polarized Sources and Targets & Polarimetry*, Ferrara, Italy, 7–11 September 2009, p. 183–192 [DOI:10.1142/9789814324922_0023].

[54] T. Maruyama et al., *A systematic study of polarized electron emission from strained gaas/gaasp superlattice photocathodes*, *Appl. Phys. Lett.* **85** (2004) 2640 [physics/0412099].

[55] W. Liu et al., *Record-level quantum efficiency from a high polarization strained GaAs/GaAsP superlattice photocathode with distributed Bragg reflector*, *Appl. Phys. Lett.* **109** (2016) 252104.

[56] J.K. Bae et al., *Improved lifetime of a high spin polarization superlattice photocathode*, *J. Appl. Phys.* **127** (2020) 124901 [arXiv:1911.09609].

[57] L. Cultrera et al., *Long lifetime polarized electron beam production from negative electron affinity GaAs activated with Sb-Cs-O: Trade-offs between efficiency, spin polarization, and lifetime*, *Phys. Rev. Accel. Beams* **23** (2020) 023401.

[58] W. Coosemans et al., *Performance of wire position sensors in a radiation environment*, in the proceedings of the *6th International Workshop on Accelerator Alignment*, Grenoble, France, 18-21 October 1999.

[59] F.J. Decker et al., *Status of the SLC linac*, in the proceedings of the *6th European Particle Accelerator Conference*, Stockholm, Sweden, 22–26 June 1998, p. 454–456.

[60] H. Matsumoto et al., *Development of C band (5712 MHz) high power waveguide components*, *Conf. Proc. C* **970512** (1997) 530.

[61] S.Y. Kazakov, *A new traveling-wave mixed-mode RF window with a low electric field in ceramic-metal brazing area*, Tech. Rep. KEK-98-120, KEK, Tsukuba (1998).

[62] S. Tokumoto et al., *High power testing results of the X band mixed mode RF windows for linear colliders*, *eConf* **C000821** (2000) THA02 [hep-ex/0008039].

[63] S. Kazakov, *High-power RF sources and components for linear colliders*, FNAL, Batavia, IL (2007).

[64] J. Qiang, *X-ray FEL linear accelerator design via start-to-end global optimization*, *Nucl. Instrum. Meth. A* **1027** (2022) 166294.

[65] J. Qiang et al., *Start-to-end simulation of the shot-noise driven microbunching instability experiment at the Linac Coherent Light Source*, *Phys. Rev. Accel. Beams* **20** (2017) 054402.

[66] J. Qiang, *Start-to-End Beam Dynamics Optimization of X-Ray FEL Light Source Accelerators*, in the proceedings of the *2nd North American Particle Accelerator Conference*, Chicago, IL, U.S.A., 9–14 Octoberr 2016, pp. 838–842 [DOI:10.18429/JACoW-NAPAC2016-WEA3IO02].

[67] J. Qiang et al., *Start-to-end simulation of x-ray radiation of a next generation light source using the real number of electrons*, *Phys. Rev. ST Accel. Beams* **17** (2014) 030701.

2023 JINST 18 P09040

[68] V. Akcelik et al., *SRF cavity imperfection studies using advanced shape uncertainty Quantification Tools*, in the proceedings of the *XXIV Linear Accelerator Conference*, Victoria, BC, Canada, 29 September–3 October 2008, pp. 870–872

[69] A. Lunin et al., *Resonant excitation of high order modes in the 3.9 GHz cavity of the Linac Coherent Light Source*, *Phys. Rev. Accel. Beams* **21** (2018) 022001.

[70] D.A. Bizzozero et al., *Multi-objective optimization with an integrated electromagnetics and beam dynamics workflow*, *Nucl. Instrum. Meth. A* **1020** (2021) 165844.

[71] ATF2 collaboration, *Experimental Validation of a Novel Compact Focusing Scheme for Future Energy-Frontier Linear Lepton Colliders*, *Phys. Rev. Lett.* **112** (2014) 034802.

[72] K. Oide, *Final focus system for linear colliders*, *AIP Conf. Proc.* **249** (1992) 518.

[73] G. White, *Reconstruction of IP Beam Parameters at the ILC From Beamstrahlung*, *Conf. Proc. C* **0505161** (2005) 1446.

[74] V.A. Alexandrov et al., *Results of final focus test beam*, *Conf. Proc. C* **950501** (1996) 2742.

[75] V. Yakimenko et al., *FACET-II facility for advanced accelerator experimental tests*, *Phys. Rev. Accel. Beams* **22** (2019) 101301.

[76] S. Riemann et al., *The ILC positron target cooled by thermal radiation*, in the proceedings of the *International Workshop on Future Linear Collider*, Strasbourg, France, 23–27 October 2017 [arXiv:1801.10565].

[77] M. Breidenbach et al., *A Concept for the ILC Positron Source*, *PoS* **ICHEP2016** (2016) 871.

[78] B. Weatherford et al., *Modular High Power RF Sources for Compact Linear Accelerator Systems*, in the proceedings of the *21st International Conference on Vacuum Electronics*, Monterey, CA, U.S.A., 19–22 October 2020, pp. 55–56 [DOI:10.1109/ivec45766.2020.9520446].

[79] B. Weatherford, E.A. Nanni and S. Tantawi, *Advanced RF Sources R&D for Economical Future Colliders*, arXiv:2203.15984.

[80] S. Belomestnykh et al., *RF Accelerator Technology R&D: Report of AF7-rf Topical Group to Snowmass 2021*, in the proceedings of the *Snowmass 2021* [arXiv:2208.12368].

[81] R.L. Ives et al., *High efficiency, low cost, RF sources for accelerators and colliders*, 2023 *JINST* **18** T05003 [arXiv:2203.12043].

[82] R. Schulte et al., *Transformative Technology for FLASH Radiation Therapy*, *Appl. Sci.* **13** (2023) 5021.

[83] S. Boucher et al., *Transformative Technology for FLASH Radiation Therapy: A Snowmass 2021 White Paper*, arXiv:2203.11047.

[84] Z.D. Farkas, *Binary Peak Power Multiplier and Its Application to Linear Accelerator Design*, *IEEE Trans. Microwave Theor. Tech.* **34** (1986) 1036.

[85] J.W. Wang et al., *Development for a supercompact X -band pulse compression system and its application at SLAC*, *Phys. Rev. Accel. Beams* **20** (2017) 110401.

[86] M. Franzi, J. Wang, V. Dolgashev and S. Tantawi, *Compact rf polarizer and its application to pulse compression systems*, *Phys. Rev. Accel. Beams* **19** (2016) 062002.

[87] https://www.varian.com/resources-support/blogs/clinical-oncology-news/3000th-truebeam-system-ships-india.

2023 JINST 18 P09040

[88] A. Cahill et al., *Measurements of Copper RF Surface Resistance at Cryogenic Temperatures for Applications to X-Band and S-Band Accelerators*, in the proceedings of the 7^{th} *International Particle Accelerator Conference*, Busan, Korea, 8–13 May, pp. 487–490 [DOI:10.18429/JACoW-IPAC2016-MOPMW038].

[89] R.A. Matula, *Electrical resistivity of copper, gold, palladium, and silver*, *J. Phys. Chem. Ref. Data* **8** (1979) 1147.

[90] A.D. Cahill et al., *High gradient experiments with X -band cryogenic copper accelerating cavities*, *Phys. Rev. Accel. Beams* **21** (2018) 102002.

[91] S. Tantawi et al., *Design and demonstration of a distributed-coupling linear accelerator structure*, *Phys. Rev. Accel. Beams* **23** (2020) 092001 [arXiv:1811.09925].

[92] E. Simakov et al., *First C-Band High Gradient Cavity Testing Results at LANL*, *JACoW* **IPAC2021** (2021) MOPAB341.

[93] E.A. Nanni et al., *Progress on the C^3 Accelerating Structure*, presented at the *US-Japan Hawaii Symposium of the US-Japan Science and Technology Cooperation Program*, 21–23 April 2021, https://conference-indico.kek.jp/event/119/page/157-poster-session.

[94] E.A. Nanni and S. Tantawi, *Update on High Gradient Research at SLAC*, talk given at the 13^{th} *Workshop on Breakdown Science and High Gradient Accelerator Technology*, 19–21 April 2021, https://indico.fnal.gov/event/22025/contributions/210700/.

[95] J. Cai, I. Syratchev and G. Burt, *Development of X band High power High efficiency Klystron*, talk given at the *CLIC RF Structure Development Meeting*, 20 January 2021, https://indico.cern.ch/event/991188/.

[96] CLIC collaboration, *The CLIC Potential for New Physics*, arXiv:1812.02093 [DOI:10.23731/CYRM-2018-003].

[97] CLIC and CLICDP collaborations, *The Compact Linear e^+e^- Collider (CLIC): Physics Potential*, arXiv:1812.07986.

2023 JINST 18 P09040